Modulation of hepatic transcription factor EB activity during cold exposure uncovers direct regulation of bis(monoacylglycerol)phosphate lipids by *Pla2g15*

Raghav Jain[1], Gisela Geoghegan[1], Jessica Davidson[1], Daniel J Nesbitt[2], Akira Abe[3], Xiaojuan Chao[5], Isabella James[1], Amy Cavanagh[1], Sylwia Michorowska[1,4], Rakesh Verma[3], Kathryn Scheuler[1], Vania Hinkoka-Galcheva[3], Evgenia Shishkova[2], Wen-Xing Ding[4], Joshua J Coon[2,6], James Shayman[3], and Judith A. Simcox[1*]

[1]Howard Hughes Medical Institute, Department of Biochemistry, University of Wisconsin-Madison, Madison, WI 53706
[2]Department of Biomolecular Chemistry, University of Wisconsin-Madison, Madison, WI 53706
[3]Department of Internal Medicine, University of Michigan, Ann Arbor, MI 48109
[4]Department of Drug Chemistry, Faculty of Pharmacy, Medical University of Warsaw, Poland
[5]Department of Pharmacology, Toxicology and Therapeutics, University of Kansas Medical Center, Kansas City, Kansas 66160
[6]Morgridge Institute for Research, Madison, WI 53715

*Correspondence: jsimcox@wisc.edu

Summary (150 words)

Cold exposure is an environmental stress that elicits a rapid metabolic shift in endotherms and is required for survival. The liver provides metabolic flexibility through its ability to rewire lipid metabolism to respond to an increased demand in energy for thermogenesis. We leveraged cold exposure to identify novel lipids contributing to energy homeostasis and found that lysosomal bis(monoacylglycerol)phosphate (BMP) lipids were significantly increased in the liver during acute cold exposure. BMP lipid changes occurred independently of lysosomal abundance but were dependent on the lysosomal transcriptional regulator transcription factor EB (TFEB). Knockdown of TFEB in hepatocytes decreased BMP lipid levels. Through molecular biology and biochemical assays, we found that TFEB regulates lipid catabolism during cold exposure and that TFEB knockdown mice were cold intolerant. To identify how TFEB regulates BMP lipid levels, we used a combinatorial approach to identify TFEB target *Pla2g15*, a lysosomal phospholipase, as capable of degrading BMP lipids in *ex vivo* liposome assays. Knockdown of *Pla2g15* in hepatocytes led to a decrease in BMP lipid species. Together, our studies uncover a required role of TFEB in mediating lipid liver remodeling during cold exposure and identified *Pla2g15* as an enzyme that regulates BMP lipid catabolism.

Keywords (10): lysosome; lipidomics; liver; cold exposure; liquid chromatography mass spectrometry (LC/MS); transcription factor EB (TFEB); phospholipase A2 G15 (Pla2g15); bis(monoacylglycero)phosphate (BMP); lysosomal phospholipase A2

Introduction

The liver maintains energy homeostasis in mammals by acting as a transistor to switch between providing glucose or lipids for peripheral tissue catabolism. In the fed state, the liver is a sink for excess glucose to maintain normoglycemia. When nutrients are scarce in fasting, the liver spares glucose for the brain and releases lipids as fuel for peripheral tissues. The shift to systemic lipid utilization is a coordinated response between multiple organs that begins with white adipose lipolysis of triglyceride stores which releases free fatty acids into circulation, a portion of which are taken up by the liver[1]. The liver processes free fatty acids into more complex lipids including triglycerides that are delivered to extrahepatic tissue. These nutrient adaptive roles establish the liver as a central regulator of systemic metabolism, and in cases of nutrient excess the metabolic flexibility of the liver is disrupted. Understanding the regulation of this fuel switch will enable treatment of diseases characterized by excess glucose and lipids including type 2 diabetes.

One mechanism to uncover the boundaries of lipid remodeling is cold exposure. Studies in cold exposure have led to the discovery that adipose triglyceride lipase, the enzyme which breaks down triglycerides to free fatty acids, is required in white but not brown adipose tissue for adaptation to cold[1,2]. This indicates that the regulation and utilization of lipid droplets is distinct in brown and white tissue with implications extending beyond cold exposure. The release of free fatty acids from white adipose alone is insufficient for cold adaptation, and processing in the liver is required for body temperature maintenance[3,4]. Acylcarnitines are one lipid class that is produced in the liver and exported into the circulation for brown adipose tissue thermogenesis[5]. These studies demonstrate that acute cold exposure is a powerful stimulus to study lipid metabolism, interorgan crosstalk, and processes that allows mammals to adapt to energy availability.

To identify other liver lipid metabolism pathways altered in cold exposure, we used untargeted liquid chromatography-mass spectrometry (LC/MS) based lipidomics. We identified over two hundred liver lipid species that were significantly altered with cold exposure[5,6]. These lipids represented a variety of chemically distinct lipid classes including acylcarnitines, triglycerides, ceramides, and phospholipids. We also noted 94 spectral features from our LC/MS analysis that were not identified but had reproducible, temperature-dependent differences in abundance. These features potentially represent unidentified lipids that mediate cold adaptation, and identifying their structure and function provides novel insights into hepatic lipid metabolism.

Using targeted lipidomics, we determined the identity of several spectral features significantly increased in liver during cold exposure as bis(monoacylglycero)phosphate (BMPs) lipids. BMP lipids are localized to lysosomes, where they are functionally

involved in mediating lipid and protein degradation[7–9]. Accumulation of BMP lipids is characteristic of a number of lysosomal disorders, however, their regulation and function remains poorly understood[10,11]. To determine if increased BMP lipids correlated with altered lysosomal function, we profiled lysosomes using imaging and biochemical assays. We observed that lysosomes were localized to lipid droplets during cold and that transcription factor EB (TFEB), a regulator of autophagy and lysosomal biogenesis, was more active in cold than RT. Liver knockdown of TFEB resulted in accumulation of liver BMPs and free fatty acids, a decrease in liver acylcarnitines, and a decrease in circulating ketone bodies. This led to cold intolerance in mice. To identify TFEB-regulated pathways important for acute cold survival, we performed ChIP-seq in the liver of RT and cold exposed mice. In cold exposure, TFEB mapped to only 5% of the total binding sites that were observed during RT. In cold exposure, there was a distinct TFEB regulatory program that led to enriched lipid metabolic pathways. We leveraged our models to determine that TFEB regulated BMP lipid levels through the lysosomal phospholipase LYPLA3 (*Pla2g15*) in hepatocytes. Our findings shed new light into the processes that govern liver adaptation to acute cold and provide novel insights into the regulation of BMP lipids via TFEB and LYPLA3, providing insight into modulation of BMP lipids for treatment of lysosomal storage disorders.

Results

Lysosomal BMP lipids are increased in the liver during cold exposure in mice.

To identify uncharacterized lipids that regulate liver fuel switching, we housed mice at room temperature (RT; 22-24°C) or cold (4°C) for 6h without food (5-6 mice/group; **Fig 1A**). Liver lipids were extracted by an organic solvent mixture and untargeted lipidomics by LC/MS was used to identify 712 lipids (**Fig S1A**). We observed that over 8000 additional MS/MS spectra collected in the experiment remained unannotated (unidentified 'features'). To determine if some of these features represented identifiable compounds important for survival in cold, we filtered the features to remove background ions and retained features that: 1) had a retention time characteristic of lipids (1.0-15min); 2) had a mass within the expected lipid range (400-1500m/z); and 3) were present in at least 80% of samples. This reduced the dataset to 1233 unidentified features (**Fig 1B**). Next, we selected lipids and unidentified spectral features based on the magnitude of fold change and significance between RT and cold using a false-discovery rate threshold of $q<0.05$ (**Fig 1C**). Features were manually identified with a focus on highly significant change between conditions and shared fragmentation patterns that suggested multiple lipids from a single class. Using the LIPIDMAPS database (https://www.lipidmaps.org), we determined that two of the most significantly increased features were bis(monoacylglycero)phosphate (BMP) lipids, a class of lysosomal lipids (**Fig S1B**).

To validate this finding, we developed a targeted LC/MS method to quantify 35 BMP lipid species and their precursor lipid phosphatidylglycerides (PGs). When summing all quantified species, total BMP lipids were not significantly ($p=0.165$) increased in cold versus RT (**Fig 1D**). However, 14 individual BMP lipids were

significantly increased in the liver during cold exposure with the majority containing essential fatty acids including 6 with an 18:2 acyl chain (**Fig 1E; Fig S1C**). The 18:2 fatty acid is a polyunsaturated fatty acid that is associated with increased membrane fluidity, potentially indicative of changes in BMP lipid function. We did not observe changes in liver PGs (**Fig S1D**). Interestingly, circulating BMP ($p<0.05$) and PG ($p<0.01$) lipids were significantly decreased during cold exposure (**Fig S1E-F**).

BMP lipids function as structural components of intralumenal vesicles within the endolysosomal system and are considered markers of lysosomal abundance. *Ex vivo* liposomal assays have demonstrated that polyunsaturation in BMP acyl chains facilitates BMP lipid interaction with lysosomal proteases and lipases, enhancing degradation of proteins and lipids in the lysosome lumen[9,12]. Since increased BMP lipid species in cold primarily contained polyunsaturated fatty acids, we next asked if changes in liver BMP lipids during cold exposure may be due to altered lysosomal function or abundance to facilitate acute cold adaptation.

Lysosomes are localized to lipid droplets during cold exposure.

To determine if the increase in BMP lipids with cold exposure was driven by increased lysosomal abundance, we evaluated protein levels of several lysosomal proteins including the membrane proteins LAMP1 and LAMP2, and the lipid hydrolase LIPA (**Fig 2A**). LAMP1, but not LAMP2, was significantly increased in cold after normalizing to loading control ($p<0.05$). The soluble lysosomal lipid hydrolase LIPA and endosomal marker RAB5A were unchanged in cold when compared to RT controls. However, the ratio of LC3BII to LC3BI, a readout of autophagic induction, was significantly increased during cold exposure ($p<0.01$).

Given the lack of correlation between BMP lipid levels and lysosomal protein abundances, we evaluated liver cathepsin B protease activity to determine if there was a difference in lysosomal function (**Fig 2B**). The mature cathepsin B protein is produced from proteolytic cleavage of procathepsin in the acidic environment of lysosomes. We found no difference in active protease due to temperature change.

We next used electron microscopy to visualized liver tissue from RT and cold exposed mice to identify potential changes in lysosomal morphology or localization. At RT, lysosomes were spread throughout hepatocytes with contacts primarily to the ER (**Fig 2C***,* top). In cold, there was a definitive change in hepatocyte morphology, characterized by increased lipid droplet abundance, elongated mitochondria, and clustering of lysosomes on lipid droplets (**Fig 2C**, bottom). In total, biochemical analysis suggested the induction of autophagy and increased lysosomal localization to lipid droplets with cold exposure.

The master lysosomal regulator transcription factor EB is activated during cold exposure.

To gain more insight into lysosomal pathways, we evaluated liver transcript levels for genes involved in lysosome biogenesis and function as well as related processes

including autophagy, mitophagy, and lipophagy (**Fig 2D; Fig S2A**). The majority of transcripts were unchanged, but the autophagosome formation-related *Sqstm* was increased in cold, supporting induction of autophagy. We also observed increased levels of several lipid droplet-associated genes including *Dgat1*, *Plin2*, and *Pnpla2*, and increased mitochondrial fatty acid oxidation-related genes including *Ppargc1a* and *Cpt1b*. *Fasn* which is involved in lipogenesis, was decreased in cold compared to RT. These observations are in agreement with previous findings[5,6].

Many transcripts related to autophagy and lysosomes contain gene sequences termed 'CLEAR' (coordinated lysosome expression and regulation) sites upstream and downstream of their promoters[13]. These sites are bound by transcription factors that are members of the MiTF (microphthalmia-associated transcription factor) family. The most abundant MiTF member in hepatocytes, the primary cell type in liver, is transcription factor EB (TFEB)[14]. TFEB is more highly detected in liver and hepatocytes of healthy humans than other MiTF members[15]. Therefore, we assessed liver protein levels of nuclear (active) versus cytosolic (inactive) TFEB in RT and cold (**Fig 2E**). The nuclear-to-cytosolic ratio of TFEB was 3-fold higher in cold than RT ($p<0.01$; **Fig 2E**).

Hepatocytes are the major liver cell type responsible for regulating circulating nutrients and 80% of liver tissue volume is composed of hepatocytes[16,17]. To determine if *Tfeb* modulated BMP lipids in hepatocytes, we used siRNA to knock down (KD) *Tfeb* in Hepa1-6 cells, a type of murine hepatocyte (**Fig S3A**). Controls were treated with siRNA containing a scramble sequence. After 48h, we harvested cells for BMP analysis and found that total BMP lipids were significantly decreased in *Tfeb* KD cells ($p<0.05$; **Fig 3A**). Moreover, knockdown of TFEB in mice in the fed state led to decreased BMP lipid levels (**Figure S3B**). These results identified TFEB as a novel genomic regulator of BMP lipids in hepatocytes. Though most studies of TFEB activity characterization have focused on lysosomal activation, previous work has implicated TFEB in the control of hepatic lipid metabolism, including through activation of *Ppargc1a*[18,19]. Given the increase in nuclear-localized TFEB and regulation of BMP lipids by TFEB in hepatocytes, we aimed to determine if TFEB was functionally important in cold tolerance.

Hepatic TFEB is required for cold tolerance in mice.

To assess the requirement of hepatic TFEB in acute cold adaptation, we knocked down *Tfeb* using shRNA encoded in an AAV8 vector which targets hepatocytes. After one week, control and KD mice were subjected to 6h at RT (23°C; n=5 and 6, respectively) while fasted, or 6h in cold (4°C; n=5 and 6, respectively) while fasted. Mice were sacrificed and *Tfeb* expression and protein abundance were measured (**Fig 3B**). In the liver, KD mice had approximately 50% lower *Tfeb* gene expression than controls, and varying levels of protein ranging from undetected to <40% signal compared to controls (**Fig 3B)**. Regardless of KD, mice kept at 4°C had significantly lower core body temperature than those at RT after 2h ($p<0.01$ at all timepoints; **Fig 3C**). However, after 4h, mice with KD had significantly lower body temperature than mice without KD at 4°C ($p<0.001$) and KD mice were unable to defend their temperature for the duration of the

experiment. These results show that hepatic TFEB is required for acute cold adaptation in mice.

TFEB KD mice have an altered liver lipidome during cold exposure.

The liver is central to defending body temperature during cold exposure due, in part, to the liver's ability to take up free fatty acids from circulation and incorporate them into triglycerides or acylcarnitines to be exported to brown adipose tissue[5]. Through untargeted lipidomics of liver tissue, we found that levels of several lipid classes were altered in KD mice kept at cold compared to controls (**Fig 3D**). Total acylcarnitines, a fuel for thermogenesis, were significantly increased in control mice kept at cold versus RT (2-3-fold increase; $P<0.01$), but this response was absent in TFEB KD mice. Concurrently, total liver free fatty acids were significantly higher in TFEB KD cold exposed mice compared to control mice in cold (2-fold increase; $P<0.001$). The acylcarnitine and free fatty acid changes occurred despite no changes in liver triglyceride content, liver weight, or body weight due to KD (**Fig 3D; Fig S3C**). These results indicated that TFEB KD altered liver lipid metabolism in a cold-specific manner. Most notably, increased free fatty acids and decreased acylcarnitines indicated that there may be less lipid energy substrates being exported by the liver to support thermogenesis. To test this hypothesis, we measured circulating lipids in control and KD mice. Unlike in the liver, total circulating acylcarnitine abundance was significantly higher in cold than RT mice regardless of KD (**Fig S3D**). The discrepancy between total liver versus circulating acylcarnitines in cold-exposed KD mice may be due to increased liver acylcarnitine export, decreased usage of circulating acylcarnitines, or compensatory production of acylcarnitines by another tissue. Circulating free fatty acids were significantly increased during cold regardless of KD, indicating adipose tissue lipolysis was functionally intact (**Fig S3D**).

In addition to conversion to acylcarnitines, free fatty acids are also catabolized into ketone bodies in the liver and exported into circulation for use in other tissues[20]. It has previously been shown that circulating ketone bodies are increased 2-fold during cold exposure in mammals[21,22]. We measured circulating ketones to determine if insufficient ketone body production may contribute to cold intolerance in TFEB KD mice. Indeed, total circulating ketone bodies were increased by nearly two-fold in plasma of control mice in cold versus RT ($P<0.001$) and this was attenuated in TFEB KD mice (**Fig 3E**). The lower ketone body formation in the TFEB KD mice with cold exposure may be driving the cold intolerance observed.

BMP lipids are increased in the liver of TFEB KD mice exposed to cold.

In cultured hepatocytes, TFEB KD decreased total BMP lipid levels (**Fig 3A**), and TFEB KD in mice in the fed state also decreased BMP lipid levels (**Fig S3B**). To determine if decreased BMP lipids were contributing to cold intolerance in TFEB KD mice, we performed targeted BMP lipid analysis on livers from control and TFEB KD mice. Total liver BMPs were significantly ($p<0.05$) increased in cold versus RT of KD mice, but not in control mice though BMPs trended towards increase in cold as well

(p=0.08; **Fig 3F**). The major BMP lipid species increased in cold were the same between WT and TFEB KD mice, with the exception of BMP 18:2_22:6 which was increased (p<0.05) in KD but not controls (**Fig 3F**). TFEB KD mice also had a decrease in BMP 20:5_22:6 (P<0.01) during cold exposure. The difference in BMP lipids in the fed and fasted state could be driven by a number of factors including loss of BMP lipids in autophagy or a change in lysosomal function.

BMP lipid abundance does not always correlate to lysosomal function[23,24]. We assessed protein levels of several endolysosomal proteins using western blot and quantified results using densitometry. There were no proteins differentially altered due to cold exposure between control and KD mice except the LC3BII-to-I ratio, which was significantly increased in cold with controls but not KD mice (**Fig S3F**). This was indicative of reduced autophagic induction in TFEB KD mice.

To gain insight into lysosomal function in lipid catabolism, we assessed the activity of lysosomal glucosylceramidase (GCase). GCase degrades glycosphingolipids to ceramides and has been shown to be dependent upon BMP lipids. GCase activity was increased in liver lysate of TFEB KD mice (**Fig S3G**). However, when we compared GCase activity to total ceramides across mice to normalize for changes in ceramide abundance (R=0.66, p=0.04), the expected positive correlation of GCase activity to ceramide levels observed in control mice was not present in TFEB KD mice (R=-0.04, p=0.92; **Fig S3G**).

These results, though modest, suggested potentially dysfunctional autophagy/lysosomal activity in TFEB KD mice. Though we had expected TFEB KD would result in a decrease in liver BMP lipids, it is possible that *in vivo*, there are other mechanisms through which BMP lipid levels are modulated. Additionally, we found that TFEB KD decreased BMP lipids in cultured hepatocytes, however the liver is composed of several other cell types including Kupffer and stellate cells, which may have contributed to higher BMP lipids during cold in TFEB KD mice.

Cold exposure rewires TFEB to coordinate lipid metabolic processes.

Given the impact of liver TFEB loss on cold tolerance and lipid profiles, we sought to understand why TFEB was required during cold exposure. Because TFEB is a transcriptional regulator, we performed ChIP-seq for TFEB in liver of mice housed at RT or fasted in cold for 6h. After filtering reads using false-discovery, we compared the number of unique genes with annotated TFEB binding sites at RT and cold (q<0.05; **Fig 4A**). Despite greater TFEB nuclear localization during cold, which is typically associated with increased activity (**Fig 2E**), TFEB was only present at 5% of the total number of DNA binding sites in cold exposure compared to RT (340 versus 6995 genes, respectively). The majority of DNA binding sites (304) were associated with similar genes at both RT and cold, and most binding sites were within 1000 base pairs of the transcriptional start site as well (**Fig S4A-B**)[25].There was a drastic shift in the type of binding sites between conditions, however, as the percentage of intronic binding sites (of total sites) decreased from 61.1% in RT to 48.4% in cold (**Fig 4B**). The greatest increase was for intergenic regions (RT 24.1% to cold 36.2%) while the percentage of

promoter binding sites were similar in both conditions (RT 7.8 and cold 6.0%). We compared our findings with previous results and found that at RT, previously published TFEB targets such as *Ctsa*, *Ctsb*, *Psap* and *Npc1* had high occupancy by TFEB (**Fig 4C**; **Fig S4C**)[13]. This was confirmed using targeted ChIP-qPCR based on binding sites annotated to TFEB from sequencing data (**Fig 4C**).

To identify the processes coordinated by TFEB in cold, we performed 'Reactome analysis' (http://geneontology.org) using genes annotated to TFEB in the cold as input and compared them to RT (**Fig S4D**). We observed that 75% of all reported Reactome processes related to lipid metabolism (**Fig 4D**). Many of the most significantly (q<0.05) enriched processes were 10-30 fold above expected representation in the gene set. With our findings from TFEB KD mice, these data indicated that TFEB is responsible for rewiring of liver lipid metabolism that occurs in cold exposure, and cold intolerance during TFEB KD may be mediated by decreased circulating ketone bodies.

TFEB regulates BMP lipids via *Pla2g15* in hepatocytes *in vitro*.

Due to the altered BMP lipid levels in TFEB KD hepatocytes, we postulated that TFEB regulates enzymes directly involved in the metabolism of BMP lipids in hepatocytes. To identify potential enzymatic BMP lipid regulators in the lysosome, we overlayed all unique genes identified in our TFEB ChIP-seq analysis with a previously published dataset of lysosomal proteins[26], and genes with expression significantly altered in cold exposure compared to RT after 6h (q<0.05; **Fig 5A** top). We filtered the resulting list of 24 genes to 4 candidates that are predicted to be regulators of lipid metabolism (**Fig 5A** bottom). Of these genes, *Pla2g15*, which encodes the protein LYPLA3 (also termed 1-O-acylceramide synthase and lysosomal phospholipase A2) emerged as a likely regulator of BMP lipids that has cold exposure dependent changes in expression. There was a sharp peak upstream of the promoter of *Pla2g15* at RT for both TFEB and RNA pol ChIP-seq – indicative of active transcription (**Fig 5B** top). There was also a CLEAR site present within the coding sequence 1543 base pairs downstream of the transcription start site (sequence: GTCACGTGTG)[25]. By performing targeted ChIP-seq for the promoter ChIP binding site, we confirmed that TFEB was bound to the promoter at RT. We also found that *Pla2g15* was more abundantly expressed at RT than cold, as was its protein product LYPLA3 (p<0.001 and p<0.05, respectively; **Fig 5B** bottom and **Fig 5C**, respectively). These data suggested that TFEB was a genomic regulator of *Pla2g15*, and the *Pla2g15*-encoded LYPLA3 protein may enzymatically regulate of BMP lipids.

LYPLA3, the protein encoded by *Pla2g15*, is a lysosome-localized enzymatic regulator of BMP lipids.

Knockdown of *Tfeb* in cultured hepatocytes led to a decrease in total BMP lipids, though *Tfeb* overexpression did not alter BMP lipids (**Fig 3A and S5A-B**). When we evaluated the expression of *Pla2g15* in *Tfeb* KD cells, we found that *Pla2g15* was

significantly increased with *Tfeb* KD ($p<0.001$; **Fig 5D**). We also took an orthogonal approach and performed a KD of mannose-6-phosphate receptor (*M6pr*), which is required to traffic LYPLA3 to lysosomes[27], and observed that total BMP lipids increased 2-fold with *M6pr* KD ($p<0.05$; **Fig S5C-D**). These data further indicated that in hepatocytes, *Tfeb* regulated BMP lipids through *Pla2g15*/LYPLA3. Lastly, we knocked down *Pla2g15* in hepatocytes using siRNA and found that several BMP lipid species were increased, including BMP 18:1_18:2, one of the primary BMP lipids increased *in vivo* with cold exposure (**Fig 5E & S5E**). These results were consistent with *Pla2g15* being a negative regulator of BMP lipids in hepatocytes.

To directly test if LYPLA3 was an enzymatic regulator of BMP lipids, we prepared liposomes containing the commercially available di-oleoyl BMP with non-hydrolyzable ether lyso-PC 18:0 in an acidic buffer to mimic the lysosome environment. We then added purified human LYPLA3 protein incubated with or without the LYPLA3 inhibitor diisopropyl fluorophosphate and monitored for the degradation product oleic acid via TLC (**Fig 5F** top). In the presence of inhibitor, there was no migration band related to oleic acid, however, in reactions containing just liposomes and LYPLA3, there was a band characteristic of oleic acid, indicating degradation of di-oleoyl BMP (**Fig 5F** bottom). Finally, *Pla2g15* expression in TFEB KD liver was significantly decreased ($p<0.05$) in TFEB KD mice kept in cold, concurrent with an increase in total and individual BMP lipid species (**Fig S5F**). Together, these data suggest that LYPLA3 is a lysosomal, enzymatic regulator of BMP lipids. LYPLA3 exerts this regulation through degradation of BMP lipids *in vitro*, and ablation of the enzyme in cultured hepatocytes results in increased levels of several BMP lipid species.

Discussion

Mammals adapt to cold temperatures by increasing thermogenesis. This requires coordination across multiple organs to increase lipid production and utilization to fuel heat production. Our studies have identified that transcription factor EB is required for acute cold adaptation in mice through coordination of lipid processing. Using biochemical and genomic analyses, we found that in cold exposure in the liver, TFEB was predominantly bound to genes associated with lipid metabolism (**Fig 4D**). Mice with liver KD of TFEB were unable to maintain their body temperature and this was associated with a decrease in liver acylcarnitines, increased liver FFAs, and decreased circulating ketone bodies (**Fig 3B-C**; **Fig 3E**). We also observed an increase of lysosomal BMP lipids in the liver of TFEB KD mice exposed to cold. BMP lipids are regulators of lysosomal lipid processing, but their regulation is poorly understood. Through *in vitro* and *in vivo* studies, we found that the lysosomal protein LYPLA3 degrades BMP lipids and that LYPLA3 expression is regulated by TFEB (**Fig 5 & S5G**). Together, these studies provide new insights into liver thermoregulatory processes and the regulation of BMP lipids. BMP lipid levels are altered in a number of human diseases including hepatic steatosis and lysosomal storage disorders, although the regulation of BMP lipids in these diseases is poorly understood.

We found a decrease in liver acylcarnitines and circulating ketone bodies in TFEB KD mice during cold exposure (**Fig S3D**), potentially indicative of mitochondrial dysfunction. However, a number of transcripts associated with mitochondrial abundance (mt*Cyb*, *mtND1-2*, and *mtAtp8*) did not have differential patterns of expression between RT and cold KD mice when compared to WT controls (**Fig S3E**). Studies in mice fasted for 24h have found that hepatic *Tfeb* expression increases by 1.5-fold and induces lipid catabolism to support energy homeostasis[19]. In those studies, TFEB-mediated activation of PGC1α drove induction of mitochondrial biogenesis, ketone body production, and fatty acid oxidation[19,28]. In our studies, liver *Ppargc1a* (PGC1α), *Hmgcs2* (the rate limiting step of ketone body formation), and *Cpt1b* (involved in acylcarnitine synthesis) were all significantly (p<0.05 for all) induced during acute cold (4°C for 6h) in TFEB KD mice at similar levels to control mice (**Fig S3E**). These data indicate that at least transcriptionally, the requirement for liver TFEB during acute cold exposure is distinct from long-term fasting. Therefore, loss of TFEB may be impacting liver mitochondrial homeostasis in ways that are not yet known. Future research should focus on tissue and context-specific activity of TFEB, particularly as TFEB activators are being explored as therapeutics for neurodegenerative diseases such as Parkinson's[29].

The most widely reported activity of TFEB is the control of autophagy and lysosomal biogenesis[13,25,30]. However, we did not observe a significant decrease in expression of lysosomal genes, including *Psap*, *Lamp1*, and *Ctsb*, in TFEB KD mice (**Fig S3E**)[13]. Protein expression of lysosomal LAMP1 was increased in TFEB KD mice kept at RT or cold when compared to RT controls, as was the endosomal marker RAB5A (p<0.05; **Fig S3F**). Coupled with higher BMP lipids in TFEB KD mice, these findings are reminiscent of lysosomal storage diseases, in which dysfunctional lysosomes accumulate lipid substrates such as glycosphingolipids due to an inability to process and degrade them[31,32]. It is possible that 1) liver TFEB KD results in loss of lysosomal function that is required for lipid metabolism to support cold tolerance; and 2) BMP lipids may be accumulating in TFEB KD liver because they are necessary, but not sufficient, to support lipid catabolism during cold adaptation. The necessity of BMP lipids is difficult to address because regulators have been poorly characterized with the exception of a recent report describing CLN5 as a BMP synthesis enzyme[33].

The resurgence in research on BMP lipids since their initial characterization in 1967 has been driven by both improved methods to detect BMP lipids[34–37], and the realization that BMP lipids are altered in metabolic[38,39] and neurodegenerative diseases[40–42]. More understanding is needed on the molecular regulation of these BMP lipids and ways in which the levels can be adjusted. We found that liver BMP lipids were significantly increased during cold exposure, and that disruption of BMP lipid levels with TFEB KD led to aberrant energy homeostasis. We went on to characterize a novel pathway of BMP lipid regulation through genetic regulation by TFEB, and enzymatic degradation of BMP lipids by LYPLA3. These findings provide valuable insight into therapeutic avenues for lysosomal diseases. For example, Ilnytska and colleagues have reported that supplementing BMP lipids to cells deficient in the cholesterol transporter NPC1 alleviates cholesterol burden and reduces cellular toxicity, which are characteristic of NPC diseases[32]. Targeting the TFEB-LYPLA3 axis may be alternative method to achieve this goal. Additionally, there are over 300 single nucleotide variants

that have been characterized for LYPLA3 encoding *Pla2g15*[43]. Identifying LYPLA3 as an enzymatic regulator of BMP lipids, which are crucial for lysosomal function, may prove crucial to understanding the implications of LYPLA3 mutants in human health and disease.

LYPLA3 was originally was originally identified by Taniyama and colleagues as a lyso-phosphatidylcholine lipase and by Abe and colleagues as a transacylase that catalyzed the formation of 1-O-acylceramides from sn-2 fatty acyl groups[44–46]. In the absence of ceramide acceptors, LYPLA3 exhibits phospholipase activity against a wide range of glycerophosphates and oxidized phospholipids[46,47]. LYPLA3 bears 50% sequence identity to LCAT, another enzyme with phospholipase A2 and transacylase activity. The enzyme contains a core α/β-hydrolytic domain and catalytic triad consisting of Ser127, Asp327, and His359. The catalytic serine is the acceptor for the fatty acyl group and is inhibited by fluorophosphonates including diisopropyl fluorophosphate[48,49]. In contrast, the recently identified BMP biosynthetic enzyme CLN5 contains a catalytic cysteine that serves as an acyl chain acceptor from lysophosphatidylglycerol (LPG) and esterifies a subsequent LPG to produce BMP lipids in lysosomes[33]. The differences in catalytic residues may underlie a key feature of enzymes that degrade BMPs (catalytic Ser) versus those capable of synthesis (catalytic Cys). This may be particularly important in the lysosomal environment which is considered predominantly catabolic and is not known to contain acyl-CoAs, the most common acyl chain donors for phospholipid synthesis[50]. *Pla2g15* is also an ortholog of the yeast autophagy gene *Atg15* and *Pla2g15* is implicated in the control of autophagy in eukaryotes[51,52]. Therefore, LYPLA3 has many other important functions in autophagic and lysosomal activity beyond the degradation of BMP lipids; these functions may be relevant for metabolic regulation in mammals and merit future studies.

A recent study reported that LYPLA3 was a regulator of BMP lipid synthesis, rather than degradation[53]. They proposed that LYPLA3 de-acylates phosphatidylglycerol at the sn-2 position in the first step of BMP lipid synthesis, and that LYPLA3 levels directly correlated with BMP lipid levels. The majority of those studies were carried out in HeLa cells. We found that murine liver LYPLA3 protein inversely correlated with BMP lipids, and siRNA mediated KD of *Pla2g15* in a murine hepatocyte cell line (Hepa1-6) increased the levels of several BMP lipid species (**Fig 5C & E**). Due to the confounding differences, we performed *ex vivo* enzymatic assays in for LYPLA3 in liposomes which demonstrate the BMP catabolic function of LYPLA3. These contradictory results may be explained by differences in cell type and specificity of LYPLA3 to particular BMP species, or substrate availability since enzymes often function bidirectionally. We found that the majority of BMP species increased when LYPLA3 was decreased contained the 18:2 acyl chain, which is poorly present in most cell culture models[54]. It is also important to note that LYPLA3-mediated synthesis of BMP would require a pool of PG lipids, which are not known to be found in lysosomes, and BMP levels could be modulated by substrate availability. Finally, there are likely other lysosomal enzymes involved in both the synthesis and breakdown of BMP lipids, highlighting the complexity of BMP regulation.

In conclusion, we found that liver TFEB is required for acute cold adaptation in mice and that the TFEB regulatory program is altered with cold exposure. TFEB mediates lipid metabolism during cold exposure and TFEB loss results in reduced lipid fuels, including ketone bodies, to support thermogenesis. We also report that TFEB mediates lysosomal BMP lipids through regulation of *Pla2g15*/LYPLA3, a lysosomal phospholipase. LYPLA3 levels were inversely correlated with BMP lipids in liver and cultured hepatocytes, and *ex vivo* data shows that LYPLA3 degrades BMP lipids. These data define new pathways in the control of mammalian thermogenesis and lysosomal lipid metabolism for future studies.

STAR Methods

REAGENT or RESOURCE	SOURCE	IDENTIFIER
Antibodies		
Rabbit anti-LYPLA3	Novus Biologicals	NBP2-17193
Rabbit anti-TFEB (western blot)	Bethyl Laboratories	A303-673A
TFEB rabbit mAb (IP)	Cell Signaling	83010
LC3B Antibody	Cell Signaling	2775
Normal Rabbit IgG	Cell Signaling	2729
Rab5a polyclonal antibody	Proteintech	11947-1-AP
LIPA polyclonal antibody	Proteintech	12956-1-AP
CD107B/LAMP2 monoclonal antibody	Proteintech	66301-1-Ig
Human/mouse/rat beta-actin antibody	R&D Systems	MAB8929
Recombinant anti-HNF-4-alpha antibody	Abcam	ab181604
Anti-LAMP1	Development Studies Hybridoma Bank, Iowa	1D4B
Goat anti-Rabbit IgG Secondary antibody HRP	Fisher Scientific	PI32460
Goat anti-Mouse IgG Secondary antibody HRP	ThermoFisher Scientific	A-10668
Goat anti-Rat IgG Secondary antibody HRP	Fisher Scientific	A10549
Bacterial and virus strains		
Biological samples		
Chemicals, peptides, and recombinant proteins		
Splash II Lipidomix	Avanti Polar Lipids	330709
14:0 BMP (S, R)	Avanti Polar Lipids	857131
18:1 BMP (S, R)	Avanti Polar Lipids	857133
18:1 (delta-9-cis) PG	Avanti Polar Lipids	840475
15:0-18:1-d7-PG	Avanti Polar Lipids	791640
15:0-18:1-d7-PA	Avanti Polar Lipids	791642
C15 Ceramide-d7 (d18:1-d7/15:0)	Avanti Polar Lipids	860681

Stearic acid-d35	Cayman Chemical	9003318
Oleoyl-L-carnitine-d3 (chloride)	Cayman Chemical	26578
Pierce Formic Acid, LC-MS Grade	ThermoFisher Scientific	85178
Acetonitrile	Honeywell	LC015
Ammonium Formate	Honeywell	55674
Water B&J Brand, LC-MS	Fisher Scientific	600-30-78
Fisher Chemical Isopropanol Optima, LC-MS	Fisher Scientific	A4614
DMEM	ThermoFisher Scientific	11-965-118
Fetal Bovine Serum (FBS)	ThermoFisher Scientific	10-437-028
DPBS	ThermoFisher Scientific	14190144
Lipofectamine RNAiMAX	ThermoFisher Scientific	13778030
Opti-MEM	ThermoFisher Scientific	31985062
Laemmli sample buffer	Bio-Rad	161-0737
β-mercaptoethanol	Sigma-Aldrich	M6250
RIPA lysis buffer	Fisher-Scientific	NC984499
Pierce protease inhibitor mini tablets, EDTA free	Fisher-Scientific	PIA32955
4-15% Mini-Protean TGX precast protein gels	Bio-Rad	4561096
PowerUp SYBR Green Master Mix	ThermoFisher Scientific	A25778
TRIzol	Invitrogen	15596018
Cathepsin B substrate III – Fluorogenic, Calbiochem	Millipore Sigma	219392
E-64-D	Enzo Life Sciences	BML-PI107-0001
Isoflurane 99.9%	McKesson	803250
25% glutaraldehyde	Electron Microscopy Sciences	16220
0.4M Sodium cacodylate	Electron Microscopy Sciences	11655
Critical commercial assays		
Glucosylceramidase activity assay kit	Abcam	ab273339
β-Hydroxybutyrate colorimetric assay kit	Cayman Chemical	700190
Wako HR Series NEFA kit	Fujifilm	999-34691; 995-34791; 991-34891; 993-35191; 276-76491; 997-76491
SimpleChIP Plus kit (Magnetic Beads) 4°C and RT reagents	Cell Signaling	#38191
Pierce Protein A/G Magnetic Beads	VWR	PI88802
Pierce BCA Protein Assay	ThermoFisher Scientific	#23225
High Capacity cDNA Reverse Transcription Kit	ThermoFisher Scientific	#4368813
Zymo ChIP DNA Clean and Concentrator Kit	VWR	D5205
Qubit dsDNA HS Assay Kit	ThermoFisher Scientific	Q32851
Agilent DNA HS Kit	Agilent Technologies	5067-4626

TruSeq ChIP Sample Preparation kit	Illumina	IP-202-1012
SuperSignal West Atto Ultimate Sensitivity Substrate	ThermoFisher Scientific	A38554
Deposited data		
Untargeted lipidomics data (WT mice)	https://doi.org/10.1016/j.jlr.2022.100197	MTBLS3730
Targeted and untargeted lipidomics of KD mice	This paper	Chorus
TFEB ChIP-seq	This paper	GEO
Experimental models: Cell lines		
Hepa1-6 cells	ATCC	CRL-1830
Experimental models: Organisms/strains		
Mouse: C57BL/6J male mice 9 weeks	Jackson Laboratories	#000664
Oligonucleotides		
ON-TARGETplus Mouse Tfeb siRNA	Dharmacon	L-050607-02-0005
ON-TARGETplus Non-targeting Control Pool	Dharmacon	D-001810-10-05
ON-TARGETplus Mouse M6pr siRNA	Dharmacon	L-050312-01-0005
ON-TARGETplus Mouse Pla2g15 siRNA	Dharmacon	L-059873-01-0005
Primers see Supplementary Table 2		
Recombinant DNA		
AAV8-GFP-U6-scrmb-shRNA	Vector Biolabs	220207-220729
AAV8-GFP-U6-mTFEB-shRNA	Vector Biolabs	220801#38
Software and algorithms		
R version 4.3.0	R Core team	https://www.r-project.org
Agilent MassHunter Suite	Agilent Technologies	G3337AA; M5960AA; M6010AA
Agilent LipidAnnotator	Agilent Technologies	G3835AA
LipidCreator	Peng *et al*.	https://doi.org/10.1038/s41467-020-15960-z
R scripts for data analysis	This paper	Github: RJain52
Other		
TissueLyser II	Qiagen	85300
Tecan Infinite M Plex	Tecan	30190085
QuantStudio 5 Real-Time PCR System	ThermoFisher Scientific	A34322
Acquity UPLC BEH C18 Column	Waters Corporation	186002352
Acquity UPLC BEH C18 VanGuard Pre-Column	Waters Corporation	1860003975
Agilent 1290 Infinity II LC System	Agilent Technologies	-
Agilent 6495c triple quadrupole mass spectrometer	Agilent Technologies	G6495CA
Agilent 6546 Q-TOF mass spectrometer	Agilent Technologies	G6546AA

iBright CL1500 Imaging System	ThermoFisher Scientific	A44240
Amersham Protran nitrocellulose blotting membrane	Fisher	45004003
Physitemp rectal probe for mouse	Fisher	NC9713069
JEM 1016CX electron microscope	JEOL Ltd.	-
Formulab Diet	LabDiet	5008

Acknowledgments

We would like to thank Edrees H. Rashan for advice on experimental design and all members of the Simcox Lab for assistance with mouse experiments and thoughtful discussions. We also thank the Lim Lab at the UW-Madison for equipment use.

Author Contributions

Conception: RJ and JAS; methodology: RJ, GG, JD, DJN, AA, AC, SM, XC, RV, IJ, KS, VHG, and ES; original draft: RJ and JAS; revisions: RJ, AC, and JAS; materials: WXD, JJC, JS, and JAS; supervision: JAS.

Declaration of Interests

The authors declare no competing interests.

Figure Legends

Figure 1. Lysosomal BMP lipids are increased in the liver during acute cold exposure in mice. A) Schematic of the experimental design to identify hepatic lipid changes during acute cold exposure in mice. B) Pie chart representing the number of identified lipids and unidentified lipid-like features from LC/MS analysis of livers. Total unidentified features (~8000) were filtered to remove background ions and contaminants and retain features present in at least 80% of samples. Remaining features were further filtered based on the retention time of lipid elution (0.5-15min) and mass-to-charge (m/z) range (200-1500m/z) of potential lipid species. C) Volcano plot of identified lipids and unidentified features (from Fig 1B) comparing RT (24°C) to cold (4°C) in the liver after 6h (n=6/group). Points in red or black represent significantly altered lipids or features, respectively, after false-discovery correction (q<0.05). Features circled in green were manually identified as lysosomal BMP lipid species based on the fragmentation pattern. D) Total BMP lipids were measured using a targeted LC/MS method in liver from RT and cold exposed mice (n=5/group). Student's t-test was used for significance testing to compare lipid values. E) Individual hepatic BMP lipid species abundances were compared. The acyl chain composition of the BMP species are plotted on the x-axes. The most abundant BMP species are plotted on the top and significantly altered (p<0.05), less abundant BMP lipids are in the bottom graph. Where relevant, mean±SD of experimental groups is plotted. *p<0.05, **p<0.01, ***p<0.001. Abbreviations: BMP,

bis(monoacylglycero)phosphate; FDR, false discovery rate; LC/MS, liquid chromatography mass spectrometry; RT, room temperature.

Figure 2. Lysosome localization is altered during cold exposure. A) Western blot of lysosomal abundance and autophagy markers in liver from RT (24°C) and cold (4°C) exposed mice (n=6/group). Densitometry based quantification was normalized to average RT signal, and Wilcoxon non-parametric test used to calculate *P*-values. B) Comparison of lysosomal cathepsin B protease activity in liver from mice at kept at RT or cold (n=6/group). C) Electron micrographs of liver sections from mice kept at either RT or cold exposure. Lysosomes are visible as dark, electron dense organelles. Arrows indicate zoomed in regions within insets. D) Schematic of potential lysosomal activities and associated genes for each process/organelle function. Genes are colored based on qPCR transcriptional changes ($p<0.05$) between RT and cold exposed murine livers (n=6/group). E) Western blot of the lysosomal regulator TFEB from liver of mice kept at RT or cold (n=6/group). Liver lysate was fractionated into nuclear and cytosolic fractions prior to western blot. Bands were quantified using densitometry and the ratio of nuclear (active) to cytosolic (inactive) TFEB signal was plotted. Where relevant, mean±SD of experimental groups is plotted. *$p<0.05$, **$p<0.01$, ***$p<0.001$. Abbreviations: RT, room temperature; TFEB, transcription factor EB.

Figure 3. Hepatic knockdown of TFEB causes cold intolerance in mice. A) Total BMP lipids of Hepa1-6 murine hepatocytes treated with siRNA against *Tfeb* or a scramble sequence control is plotted (n=3/group). B) Western blot for TFEB in mice treated with AAV8-GFP-U6-scrmb-shRNA (control; n=10) or AAV8-GFP-U6-TFEB-shRNA (TFEB knockdown; n=12) two weeks after AAV injection to knockdown (KD) TFEB in murine hepatic tissue and cold tolerance test. Underneath the western blot, qPCR data on expression of hepatic Tfeb is shown (n=2 replicates/mouse). C) Core body temperature was measured hourly via rectal probe in control or TFEB KD mice kept at RT (n=5 and 6, respectively) or cold (4°C; n=5 and 6, respectively) for 6h. A two-way ANOVA with interaction was used to assess the effect of KD and environmental temperature on core body temperature. Asterisks (*) denote significant ($p<0.05$) difference between core temperature due to temperature of mice with the same KD status. Pound sign (#) indicates significant difference in core temperature between control and KD mice kept at 4°C. D) Lipid abundance of various lipid classes in in the liver are measured by untargeted LC/MS lipidomics are plotted. Values are relative to RT controls ('Con_RT') for each lipid class. n=5-6 per group. E) Circulating ketones were measured in mice with or without TFEB knockdown (KD). F) Total liver BMP lipids for each group from the cold tolerance test (n=5-6/group) by targeted lipidomics. Abundant, BMP lipid species significantly altered during cold exposure are plotted (n=5-6/group). Where relevant, mean±SD of experimental groups is plotted. *$p<0.05$, **$p<0.01$, ***$p<0.001$. Abbreviations: ACar, acylcarnitines; BHB, β-hydroxybutyrate; BMP, bis(monoacylglycero)phosphate; Con, control; FFA, free fatty acids; KD, knockdown; LC/MS, liquid chromatography mass spectrometry; RT, room temperature; TFEB, transcription factor EB; TG, triglycerides.

Figure 4. ChIP-seq of hepatic TFEB indicates a reprogramming towards lipid metabolism during cold exposure. A) Venn diagram comparing hepatic TFEB binding sites to unique genes between RT and cold based on ChIP-seq. B) Pie chart describing the distribution of TFEB genomic binding sites during RT or cold. C) ChIP tracks of previously described genes known to be bound by TFEB are shown[13]. Targeted ChIP-qPCR was performed to validate binding sites at regions marked by red pound signs on the ChIP tracks. D) Reactome of genes annotated to TFEB binding sites during cold exposure. Of the twenty general processes represented in the gene set, those related to lipid metabolism are annotated with a '#'. All ChIP analyses were performed after false-discovery correction with a $q<0.05$ cutoff. Where relevant, mean±SD of experimental groups is plotted. *$p<0.05$, **$p<0.01$, ***$p<0.001$. Abbreviations: ChIP-seq, chromatin immunoprecipitation sequencing; RT, room temperature

Figure 5. *Pla2g15*/LYPLA3 is a lysosomal enzymatic regulator of BMP lipids in hepatocytes. A) Overlay of identified lysosomal proteins from Eapen *et al.* (2021)[26] with all unique genes from TFEB ChIP-seq ($q<0.05$) and all genes with expression significantly altered between RT and cold after 6h ($q<0.05$). Of the 24 genes in the center overlap, four were annotated with lipid functions and are shown in the table. B) ChIP tracks of TFEB and RNA polymerase on the genomic region encoding *Pla2g15* in RT and cold livers. Underneath, targeted ChIP-qPCR is shown for the binding regions of TFEB to regions of *Pla2g15*. Additionally, gene expression, measured by qPCR, is shown for *Pla2g15* in RT and cold exposed livers (n=6/group, two replicates per sample). C) Western blot of LYPLA3, the protein encoded by *Pla2g15*, is shown for RT and cold exposed mice (n=6/group). Band intensity, normalized to the loading control b-actin, is plotted. D) Gene expression of *Pla2g15* in Hepa1-6 cells treated with siRNA targeting Tfeb or scramble sequence as control (n=3/group, 2 replicates per sample). E) Schematic of an in-vitro liposome assays using commercially available di-oleoyl BMP that was used to assess LYPLA3 activity. The expected product from LYPLA3 degradation of di-oleoyl BMP was oleic acid. The LYPLA3 inhibitor diisopropyl fluorophosphate was used as negative control. Underneath, a TLC plate with results of the assay is shown. The band related to oleic acid migrating after release from BMP is labeled (n=4/group). F) Select BMP lipid species were measured from Hepa1-6 cells following treatment with siRNA against *Pla2g15* or a scramble sequence control (n=5/group). Abbreviations: BMP, bis(monoacylglycero)phosphate; TFEB, transcription factor EB.

Supplementary Figures

Figure S1. BMP lipids are altered during acute cold exposure in the liver and in circulation in mice. A) Chromatograph traces of untargeted, LC/MS-based lipidomics is shown for liver. Identified lipid classes are labeled above the chromatographic regions of elution, with lipids predominantly identified in positive ionization in orange, and negative ionization in brown. B) Chromatographic separation and fragmentation spectra and structures of isomeric BMP and PG species containing 18:1/18:1 acyl chains are

shown. Standards were purchased from Avanti Polar Lipids. A targeted LC/MS method was developed to distinguish and quantify BMP and PG species. C) BMP lipid species unchanged between RT (fasted for 6h) and cold exposed (4°C for 6h) male mice (n=5-6/group) are shown. D) Total and individual PG species from liver measurements of the same mice as in Fig S1B are shown. E) Changes in total plasma BMP and PG lipids for mice from Fig S1B are plotted. F) Changes in BMP and PG individual lipid species from SFig 1E are shown. *p<0.05, **p<0.01, ***p<0.001. Abbreviations: BMP, bis(monoacylglycero)phosphate; FDR, false discovery rate; LC/MS, liquid chromatography mass spectrometry; PG, phosphatidylglycerol; RT, room temperature.

Figure S2. Liver transcripts of lysosome-associated processes are altered during acute cold. A) Data for all transcripts measured in Fig 2D are plotted. Mice were fasted and kept at either RT or cold (4°C) for 6h. Gene expression was measured for 4-6 mice/group with two technical replicates for all measurements and only transcripts with CT values < 30 were reported. *p<0.05, **p<0.01, ***p<0.001. Abbreviations: RT, room temperature.

Figure S3. TFEB liver knockdown caused lysosomal alterations and changes in circulating fuel, leading to cold intolerance. A) Gene expression of *Tfeb* in Hepa1-6 cells treated with siRNA targeting *Tfeb* or a scramble sequence as control is shown. Western blot of TFEB protein is shown underneath (n=3/condition for all). B) Total liver BMP lipids were measured from male B6 mice treated with an AAV8 harboring shRNA to *Tfeb* or scramble sequence as control. Mice were housed at RT and with *ad libitum* access to food and water prior to measurements (n=5/group). C) Body weight was measured before and after mice treated with control or an AAV8 virus with shRNA targeting Tfeb were housed at RT or cold (4°C) for 6h (n=5-6/group). Change in body weight was compared (left), as well as wet liver weight (right) at the end of the experiment. D) Circulating acylcarnitines (left) and free fatty acids (right) were measured in mice from Fig S3C. E) Gene expression of liver transcripts related to mitochondrial and lysosomal abundance and activity were measured in mice. Technical replicates were assessed for all transcripts. F) Protein expression of lysosome and autophagy-related proteins was assessed in the liver of mice from Fig S3A using western blot. Densitometry results are plotted. G) An *in vitro* assay to measure liver GCase, a lysosomal lipid hydrolase, was used to assess lysosomal activity in mice from Fig S3C. Total hepatic ceramides, measured by untargeted lipidomics, are correlated with lysosomal GCase enzyme activity, which produces ceramides from more complex sphingolipids. A line of best fit is plotted to the data with 95% confidence intervals shaded control (black line) and KD (grey line) mice. The Spearman correlation coefficients and p-values are provided. Each point represents a different mouse, shaded by KD and environmental temperature status (n=5-6/group). *p<0.05, **p<0.01, ***p<0.001. Abbreviations: AAV8, adeno-associated virus serotype 8; ACars, total acylcarnitines; GCase, glucosylceramidase; RT, room temperature; TFEB, transcription factor EB.

Figure S4. ChIP-seq of liver TFEB indicates a unique program during cold exposure. A) Histograms comparing the distance from transcription start sites (TSS) of ChIP-seq

analysis of liver TFEB from RT and 6h fasted, cold-exposed (4°C) mice was compared (q<0.05 for all sites used in comparison). B) The type of gene associated to TFEB binding sites in RT (top) or cold (bottom) were compared. C) Targeted ChIP-qPCR was performed on lipid metabolism-associated genes with TFEB binding site from ChIP-seq analysis was used to validate findings. TFEB ChIP-qPCR from liver (n=2) was compared to IgG (n=2) for validation. Relative enrichment of target binding sites is shown on the left with the associated ChIP tracks on the right. An arrow denotes the binding region for which qPCR primers were designed. D) GO analysis was performed using a gene list of all genes uniquely mapped to TFEB binding sites at RT (q<0.05 for binding). *p<0.05, **p<0.01, ***p<0.001, ****p<0.0001. Abbreviations: ChIP, chromatin immunoprecipitation and sequencing; GO, gene ontology; RT, room temperature; TFEB, transcription factor EB.

Figure S5. *Pla2g15*/LYPLA3 is an enzymatic regulator of BMP lipids in Hepa1-6 hepatocytes. A) Gene expression of human *Tfeb* (h*Tfeb*) in Hepa1-6 cells with retroviral overexpression of *hTfeb* or *LacZ* as control (n=6/group). B) Human *Tfeb* was overexpressed in Hepa1-6 cells and total BMP lipids were measured (n=6/group). Total BMPs were normalized to protein amount from cells. C) Gene expression of mouse *M6pr* in Hepa1-6 cells treated with siRNA containing a scramble sequence or targeting murine *M6pr* (n=4/group; technical replicates). D) Total BMP lipids were measured in Hepa1-6 cells treated with siRNA with scramble sequence (n=3) or murine *M6pr* (n=5), which traffics lysosomal protein including LYPLA3 to lysosomes. Lipid data was normalized to total protein. E) Gene expression of mouse *Pla2g15* in Hepa1-6 cells treated with siRNA containing a scramble sequence or targeting murine *Pla2g15* (n=3/group; technical replicates). F) Gene expression of *Pla2g15* in liver of mice treated with control or AAV8 with shRNA targeting *Tfeb* and housed at RT or cold (4°C) for 6h while fasted was assessed (n=5-6/group; technical replicates). G) A model is proposed to describe the regulation of BMP lipids by TFEB and *Pla2g15*. Abbreviations: BMP, bis(monoacylglycero)phosphate; KD, knockdown; *M6pr*, mannose-6-phosphate receptor; RT, room temperature; TFEB, transcription factor EB.

Supplementary Tables

Table S1. Relative lipid amounts for all LC-MS data.

Tables S2. Sequences for all qPCR primers.

Method Details

Mouse husbandry

Animals were housed in accordance with approved IACUC protocols at the University of Wisconsin-Madison. Mice were housed at room temperature using 12h dark and light cycles. Mice had *ad libitum* access to water and standard chow prior to experiments.

Cold tolerance test

Male C57Bl/6J mice (10-12 weeks old) were fasted without bedding at room temperature (RT; 22°C) or cold (4°C) with *ad libitum* access to water (n=5-6/group). Temperature was taken hourly via rectal probe and mice were monitored for any changes in behavior or physiology. Experiments started at zeitgeber time=3. After 6h, mice were sacrificed using isoflurane. Plasma was obtained via cardiac puncture. Post-isoflurane and cervical dislocation, tissue was harvested, washed with PBS, sectioned and either flash frozen in liquid nitrogen or further processed depending on subsequent analyses.

AAV injection

For WT and *Tfeb* KD experiments, littermate controls were used and mice were age and weight-matched. Mice were retro-orbitally injected with the appropriate AAV at 5e11 genome copies/mouse (mice weighing 23-28g). Post-injection weights were monitored to ensure no deviation between groups and that no more than 20% body weight was lost post-injection. Three days following injection, mouse bedding was changed to dispose of shed virus. Subsequent experiments were performed one week after injections.

Cell culture

Hepa1-6 cells were cultured at 5% CO_2 at 37°C. Cells were maintained in DMEM with 4.5 g/L glucose, supplemented with 10% fetal bovine serum. For knockdown of *Tfeb* and *Pla2g15*, ON-TARGETplus Mouse Tfeb pooled siRNA was purchased from Horizon Discovery. Transfection was performed in Hepa1-6 cells in a 6-well plate using 50 pmol siRNA and Lipofectamine RNAiMAX according to the manufacturer's instructions. Briefly, 5e5 cells were plated per well in a 6-well culture plate. Cells were cultured in DMEM+10% FBS overnight. The next day, media was replenished and a mixture of 300µL Opti-MEM with 9uL lipofectamine agent and appropriate siRNA was added to wells. Media was replenished 24h later to remove siRNA, then harvested after an additional 24h of culturing.

RNA extraction and RT-PCR

RNA was recovered from tissues or cells with TRIzol reagent followed by homogenization using TissueLyser. cDNA was synthesized using High-Capacity cDNA Reverse Transcription Kit. RT-PCR amplification was for 40 cycles using PowerUp SYBR Green Master Mix in a 384-well plate using QuantStudio 5 Real-Time PCR System. Primer sequences are listed in **Table S2**. For quantification, a standard curve was generated for each primer set and used to determine relative gene expression. Expression levels are presented relative to the housekeeping gene *Rps3*.

ChIP-seq

Chromatin immunoprecipitation was performed on livers from individually housed male C57BL/6J mice (11 weeks old) that were placed at 4°C without food for 6 hours or kept at RT with ad libitum access to food (n=2 per group). All mice had ad libitum access to water. SimpleChIP Plus Enzymatic Chromatin IP Kit was used according to

manufacturer's instructions. Briefly, 100mg of tissue was used per mouse and two immunoprecipitations were performed with rabbit anti-TFEB antibody, and two immunoprecipitations were performed wtih normal rabbit IgG control. ChIP DNA was purified using Zymo ChIP DNA Clean and Concentrator Kit. Purified immunoprecipitated and input DNA was quantified and assessed for sheering using the Qubit dsDNA HS Assay Kit and Agilent DNA HS chip, respectively. Samples were prepared according the TruSeq ChIP Sample Preparation kit. Libraries were size selected for an average insert size of 350 bp using SPRI-based bead selection. Quality and quantity of the finished libraries were assessed using an Agilent Tapestation and Qubit dsDNA HS Assay Kit, respectively. Paired end 150bp sequencing was performed on the NovaSeq 6000 by the UW-Madison Biotechnology Center.

Sequenced reads were checked for: sequencing quality, insert length, read concordance, duplications, and adapters via FastP and then aligned to the mouse genome (UCSC build mm10) via bowtie2 v2.2.5 using the sensitive end-to-end read alignment mode. Aligned reads are sorted and indexed with SAMtools 1.9 and peaks are called at $p \leq 0.05$ and $q \leq 0.05$ (separately) using the input/IgG as the background control with the MACS2. Primary and differential peaks were annotated for their positioning relative to genomic elements with Homer v4.11. *De novo* and known motif analysis were carried out with Homer. Raw data are deposited in GEO datasets.

Western blot

Tissue (25-50mg) was homogenized in a round bottom microfuge tubes containing a single steel bead in RIPA buffer with protease inhibitor using the TissueLyzer II. Lysate was centrifuged at 4°C for 10min at 14000 RPM and the supernatant was transferred to a new tube. BCA assay was used to determine protein concentration, then samples were prepared at a concentration of 2mg/mL in Laemmli sample buffer containing 5% β-mercaptoethanol. Samples were heated at 95°C for 5min, then 15-30ug protein were loaded into precast gels. Gels were run at 150V for 30-45min, then transferred at 100V for 75min onto nitrocellulose membranes.

Membranes were blocked in either 5% milk or 5% BSA, per manufacturer instructions, prior to overnight incubation in the appropriate primary antibody at 1:1000 dilution in blocking buffer, overnight at 4°C. Secondary antibodies were diluted at 1:5000 in blocking buffer and incubation was performed for 1h at RT, then membranes were developed using ECL reagent. Blots were imaged and densitometry was performed on an iBright CL1500 imaging system.

Electron microscopy

Mice were sacrificed using isoflurane and cervical dislocation, the liver was immediately perfused with 30mL PBS, followed by the fixation buffer containing 2.5% glutaraldehyde in 0.4M sodium cacodylate (pH=7.4). The liver was excised, submerged in fixation buffer, and cut into small pieces before being placed in fresh fixation buffer overnight at 4°C. The following day, samples were transferred to 15mL tube containing fresh fixation buffer and further processed for imaging. Images were collected on a JEM 1016CX electron microscope[55].

Lipid extraction

Murine tissue were extracted for lipids using a one-phase method as previously described[6]. For liver, 25-30mg tissue were homogenized in ceramic bead tubes in a 3:1:6 IPA:H_2O:$EtOAc^-$ solution containing the following internal standards (IS): 12uL of SPLASH II LipidoMix and 10µl of 10uM PG 15:0/18:1_{d7}, 10uM BMP 14:0_14:0, 30uM Cer d18:1_15:0_{d7}, 30uM ACar 18:1_{d3}, 225uM C18:0_{d35}, and 1.1mM PA 15:0/18:1_{d7}. A TissueLyser II was used for bead beating. Homogenates were incubated at -20°C for 10min, then centrifuged at 16,000xg for 10min at 4°C to precipitate protein before the lipid containing solvent layer was transferred to a new tube. Samples were respun as previously to precipitate remaining debris, transferred to another tube, then dried down in a SpeedVac. Lipid extracts were resuspended in 150µl 100% MeOH for negative or 9:1 MeOH:toluene for positive ionization analysis. Plasma samples were extracted identically expect 50µl plasma were used as starting material. Samples were transferred for autosampler vials containing glass inserts for analysis.

Samples from cell culture were prepared by first aspirating media, washing twice with DPBS on ice, then gently scraping samples into 1mL DPBS and transferring to a microfuge tube. After pelleting the samples and aspirating DPBS, 100% MeOH containing IS as above was added to samples for lipid extraction. Cell pellets were dispersed with light vortexing and incubated on ice for 1h, with additional vortexing every 15min. Following centrifugation at 16,000xg for 15min to pellet protein and cell debris, the lipid containing liquid phase was transferred to a new tube. Extracts were respun to pellet remaining debris, then transferred to autosampler vials with insert for analysis.

Untargeted lipidomics

Lipid extracts were analyzed as previously described[6]. Briefly, an Agilent 1290 Infinity II liquid chromatograph (LC) coupled to an Agilent 6546 quadrupole time-of-flight mass spectrometer (MS) was used for untargeted analyses. Lipids were separated using a Waters Acquity BEH C18 column (1.7µm, 2.1x100mm) held at 50°C. Mobile phase A was 60:40 MeCN:H_2O and B was 9:1:90 MeCN:H_2O:IPA, both with 0.1% (v/v) formic acid and 10mM ammonium formate, using the following gradient: 15% mobile phase B to 30% at 2.40min, to 48% at 3min, to 82% at 13.2min, finally to 99% from 13.2 to 13.8min held until 15.4 min before re-equilibration to 15% at a constant 0.500mL/min. Samples were analyzed in positive and negative ionization as separate experiments. All samples were injected undiluted at 10µl volumes for negative mode. For positive ionization, samples were diluted 20 to 40-fold (after evaluating saturation) and injected between 1-3uL.

Libraries of identified lipids were created using pooled samples and collecting MS/MS spectra on 6 consecutive injections using iterative exclusion. Agilent LipidAnnotator was used for lipid annotation, then individual samples were analyzed using MS1 acquisition and peak integration was performed in Agilent Profinder using mass and retention time from the lipid libraries. Subsequent steps including normalization to IS was performed in R using publicly available custom scripts (https://github.com/RJain52/Multi-Tissue-Cold-Exposure-Lipidomics).

Targeted BMP and PG lipid measurements

A targeted BMP and PG LC/MS method was developed using an Agilent 1290 Infinity I LC coupled to an Agilent 6495c triple-quadrupole MS. Lipids were extracted using a one-phase extraction (see *Lipid extraction*)[34,38]. An *in-silico* multiple reaction monitoring (MRM) method was developed using LipidCreator for fragmentation patterns of BMP and PG of different acyl chain configurations in positive ($[M+H]^+$ and $[M+NH4]^+$ adducts) and negative ($[M-H]^-$) ionization[56]. Samples were then injected using the same LC parameters as *Untargeted lipidomics* using the MRM methods. BMP lipids eluted 0.3-1min earlier than the PG species of the same acyl chains, depending on the species. This pattern was confirmed using BMP 18:1_18:1 and PG 18:1_18:1 standards purchased from Avanti Polar Lipids. Additionally, BMP(s) had unique fragments in positive ionization when compared to PG(s) of the same species. No unique fragments were observed in negative ionization; however the acyl chain carbon lengths were discernable, and ion signals were much higher due to the physicochemical properties of BMP and PG. Therefore, we created a negative mode dynamic MRM (dMRM) method for all identifiable BMP and PG species using retention time information from positive ionization, in which we could distinguish isomeric BMP and PG species via fragmentation, but scanning for precursor/products providing acyl chain information. For all subsequent analyses, pooled extracts were run in positive and negative ionization to allow for manual verification of lipid identity and individual samples were run only using negative mode dMRM analysis. Non-endogenous BMP 14:0/14:0 and PG $15:0/18:1_{d7}$ were used as IS. Data was processed in Agilent MassHunter Quantitative Analysis prior to downstream analyses in R.

Non-esterified fatty acid measurements

Plasma non-esterified fatty acids were measured using a colorimetric assay on a Tecan plate reader according to manufacturer's instructions. A five-point standard curve (0~2.5 mM) of non-esterified oleic acid standard was used to calculate NEFA concentration from 2µl plasma. Samples were analyzed in duplicate.

Ketone body assay

Plasma ketone bodies were measured by colorimetric assay using the manufacturer protocol. Briefly, 40µl plasma were diluted with 60µl assay buffer then duplicate wells for each sample were prepped with 50µl diluted plasma/well. Reaction was initiated and allowed to run for 30min at RT in the dark, then read using a Tecan plate reader at an absorbance of 445nm.

Cathepsin B assay

Cathepsin B was assayed as previously described[30]. Briefly, 15mg liver was homogenized in 300µl lysis buffer (50mM Tris, 130mM NaCl, 10% (v/v) glycerol, 0.5% (v/v) NP-40, 0.5mM EDTA, 0.5mM EGTA, 1mM PMSF; pH=7.4) using sonication (Branson Sonifier 450) (60% duty cycle; output=4) on ice. Protein content was measured using BCA assay, then 15ug protein was incubated with 50uM Cathepsin B substrate. Reactions were conducted in the presence and absence of the cathepsin B inhibitor E-64-D in assay buffer (100mM NaCl, 100mM sodium acetate; pH=5.5) at a final volume of 100µl for 30min at $37^{o}C$. Activity was based on fluorescence of cleaved substrate measured at an excitation/emission of 355/460nm.

Glucosylceramidase activity assay

A fluorometric assay to measure glucosylceramidase activity was performed using the manufacturer protocol. Briefly, 10-12mg liver was homogenized in 200µl assay buffer by glass 2mL dounce. 5µL of lysate was used to assay for enzyme activity. Reactions were incubated in the dark at 37°C for 30min before quenching. Fluorescence was measured at an excitation/emission of 360/445nm at 37°C. Remaining lysate was used to measure protein concentration for normalization using BCA assay.

Liposome assay

Liposome assays were carried out as previously described[57]. Briefly, 3,3'-(S,S)-BMP (C18:1,C18:1)/1,2-O-octadecenyl-sn-glycero-3- phosphocholine (non-substrate of LPLA2) liposomes were prepared by mixing reagents in a glass tube and drying down under N_2. Lipid mixture was dispersed in a 50mM sodium citrate solution (pH=4.5) using sonication. Reactions contained liposomes and either sucrose buffer, sucrose buffer with human LYPLA3, or sucrose buffer with DFP-treated human LYPLA3, incubated at 37°C for 10min. Reactions were quenched with 2:1 chloroform:MeOH, then 0.9% (w/v) NaCl solution causing phase separation of a top aqueous and bottom lipid containing layer. The lipid layer was transferred to glass tubes, dried down under N_2, and developed using thin-layer chromatography with a solvent system of 90:10 (v/v) chloroform:acetic acid to separate lipid fractions. Bands corresponding to lipid fractions were visualized using and 8% (w/v) $CuSO_4$ solution with 6.8% (v/v) H_3PO_4 and 32% (v/v) MeOH.

Statistical analyses

Analyses were conducted using R unless otherwise stated. Where relevant, mean±SD were reported. For comparisons between two groups, Student's t-test was used and a *p*-value less than 0.05 was considered significant, unless otherwise stated. For untargeted analyses, false-discovery correction was used an $q<0.05$ was considered significant. For comparisons of >2 groups, ANOVA analysis was used to test for significance followed by pairwise t-tests. All scripts used for analysis are freely available on Github (username: RJain52).

References

1. Haemmerle, G., Lass, A., Zimmermann, R., Gorkiewicz, G., Meyer, C., Rozman, J., Heldmaier, G., Maier, R., Theussl, C., Eder, S., et al. (2006). Defective Lipolysis and Altered Energy Metabolism in Mice Lacking Adipose Triglyceride Lipase. Science *312*, 734–737. 10.1126/science.1123965.

2. Schreiber, R., Diwoky, C., Schoiswohl, G., Feiler, U., Wongsiriroj, N., Abdellatif, M., Kolb, D., Hoeks, J., Kershaw, E.E., Sedej, S., et al. (2017). Cold-Induced Thermogenesis Depends on ATGL-Mediated Lipolysis in Cardiac Muscle, but Not Brown Adipose Tissue. Cell Metab. *26*, 753-763.e7. 10.1016/j.cmet.2017.09.004.

3. Geoghegan, G., Von Bank, H., Jain, R., Gonzalez, P., Hurtado-Thiele, M., Kirsh, C., Huck, I., Apte, U., Attie, A., Keller, M., et al. (2022). Hnf4 A Regulates Hepatic Peroxisomal Biogenesis and Fatty Acid Elongation During the Thermogenic Response. 10.2139/ssrn.4063231.

4. Sostre-Colón, J., Uehara, K., Garcia Whitlock, A.E., Gavin, M.J., Ishibashi, J., Potthoff, M.J., Seale, P., and Titchenell, P.M. (2021). Hepatic AKT orchestrates adipose tissue thermogenesis via FGF21-dependent and -independent mechanisms. Cell Rep. *35*, 109128. 10.1016/j.celrep.2021.109128.

5. Simcox, J., Geoghegan, G., Maschek, J.A., Bensard, C.L., Pasquali, M., Miao, R., Lee, S., Jiang, L., Huck, I., Kershaw, E.E., et al. (2017). Global analysis of plasma lipids identifies liver-derived acylcarnitines as a fuel source for brown fat thermogenesis. Cell Metab. *26*, 509-522.e6. 10.1016/j.cmet.2017.08.006.

6. Jain, R., Wade, G., Ong, I., Chaurasia, B., and Simcox, J. (2022). Determination of tissue contributions to the circulating lipid pool in cold exposure via systematic assessment of lipid profiles. J. Lipid Res., 100197. 10.1016/j.jlr.2022.100197.

7. Rodriguez-Navarro, J.A., Kaushik, S., Koga, H., Dall'Armi, C., Shui, G., Wenk, M.R., Di Paolo, G., and Cuervo, A.M. (2012). Inhibitory effect of dietary lipids on chaperone-mediated autophagy. Proc. Natl. Acad. Sci. *109*, E705–E714. 10.1073/pnas.1113036109.

8. Locatelli-Hoops, S., Remmel, N., Klingenstein, R., Breiden, B., Rossocha, M., Schoeniger, M., Koenigs, C., Saenger, W., and Sandhoff, K. (2006). Saposin A mobilizes lipids from low cholesterol and high bis(monoacylglycerol)phosphate-containing membranes: patient variant Saposin A lacks lipid extraction capacity. J. Biol. Chem. *281*, 32451–32460. 10.1074/jbc.M607281200.

9. Kirkegaard, T., Roth, A.G., Petersen, N.H.T., Mahalka, A.K., Olsen, O.D., Moilanen, I., Zylicz, A., Knudsen, J., Sandhoff, K., Arenz, C., et al. (2010). Hsp70 stabilizes lysosomes and reverts Niemann–Pick disease-associated lysosomal pathology. Nature *463*, 549–553. 10.1038/nature08710.

10. Akgoc, Z., Sena-Esteves, M., Martin, D.R., Han, X., d'Azzo, A., and Seyfried, T.N. (2015). Bis(monoacylglycero)phosphate: a secondary storage lipid in the gangliosidoses. J. Lipid Res. *56*, 1006–1013. 10.1194/jlr.M057851.

11. Showalter, M.R., Berg, A.L., Nagourney, A., Heil, H., Carraway, K.L., and Fiehn, O. (2020). The Emerging and Diverse Roles of Bis(monoacylglycero) Phosphate Lipids in Cellular Physiology and Disease. Int. J. Mol. Sci. *21*, 8067. 10.3390/ijms21218067.

12. Oninla, V.O., Breiden, B., Babalola, J.O., and Sandhoff, K. (2014). Acid sphingomyelinase activity is regulated by membrane lipids and facilitates cholesterol transfer by NPC2. J. Lipid Res. *55*, 2606–2619. 10.1194/jlr.M054528.

13. Sardiello, M., Palmieri, M., di Ronza, A., Medina, D.L., Valenza, M., Gennarino, V.A., Di Malta, C., Donaudy, F., Embrione, V., Polishchuk, R.S., et al. (2009). A gene network regulating lysosomal biogenesis and function. Science *325*, 473–477. 10.1126/science.1174447.

14. Azimifar, S.B., Nagaraj, N., Cox, J., and Mann, M. (2014). Cell-type-resolved quantitative proteomics of murine liver. Cell Metab. *20*, 1076–1087. 10.1016/j.cmet.2014.11.002.

15. Dynamic human liver proteome atlas reveals functional insights into disease pathways (2022). Mol. Syst. Biol. *18*, e10947. 10.15252/msb.202210947.

16. Gates, G.A., Henley, K.S., Pollard, H.M., Schmidt, E., and Schmidt, F.W. (1961). The cell population of human liver. J. Lab. Clin. Med. *57*, 182–184. 10.5555/uri:pii:0022214361900646.

17. R Daoust (1958). The cell population of liver tissue and the cytological reference bases. Am Inst Biol Sci *Liver Function*.

18. Gosis, B.S., Wada, S., Thorsheim, C., Li, K., Jung, S., Rhoades, J.H., Yang, Y., Brandimarto, J., Li, L., Uehara, K., et al. (2022). Inhibition of nonalcoholic fatty liver disease in mice by selective inhibition of mTORC1. Science *376*, eabf8271. 10.1126/science.abf8271.

19. Settembre, C., De Cegli, R., Mansueto, G., Saha, P.K., Vetrini, F., Visvikis, O., Huynh, T., Carissimo, A., Palmer, D., Jürgen Klisch, T., et al. (2013). TFEB controls cellular lipid metabolism through a starvation-induced autoregulatory loop. Nat. Cell Biol. *15*, 647–658. 10.1038/ncb2718.

20. Puchalska, P., and Crawford, P.A. (2017). Multi-dimensional Roles of Ketone Bodies in Fuel Metabolism, Signaling, and Therapeutics. Cell Metab. *25*, 262–284. 10.1016/j.cmet.2016.12.022.

21. Iossa, S., Barletta, A., and Liverini, G. (1994). Different effects of cold exposure and cold acclimation on rat liver mitochondrial fatty acid oxidation and ketone bodies production. Int. J. Biochem. *26*, 425–431. 10.1016/0020-711x(94)90063-9.

22. Bornstein, M.R., Neinast, M.D., Zeng, X., Chu, Q., Axsom, J., Thorsheim, C., Li, K., Blair, M.C., Rabinowitz, J.D., and Arany, Z. (2023). Comprehensive quantification of metabolic flux during acute cold stress in mice. Cell Metab. 10.1016/j.cmet.2023.09.002.

23. Kobayashi, T., Beuchat, M.-H., Lindsay, M., Frias, S., Palmiter, R.D., Sakuraba, H., Parton, R.G., and Gruenberg, J. (1999). Late endosomal membranes rich in lysobisphosphatidic acid regulate cholesterol transport. Nat. Cell Biol. *1*, 113–118. 10.1038/10084.

24. Hein, L.K., Duplock, S., and Fuller, M. (2013). Selective reduction of bis(monoacylglycero)phosphate ameliorates the storage burden in a THP-1 macrophage model of Gaucher disease. J. Lipid Res. *54*, 1691–1697. 10.1194/jlr.M038232.

25. Palmieri, M., Impey, S., Kang, H., di Ronza, A., Pelz, C., Sardiello, M., and Ballabio, A. (2011). Characterization of the CLEAR network reveals an integrated control of cellular clearance pathways. Hum. Mol. Genet. *20*, 3852–3866. 10.1093/hmg/ddr306.

26. Eapen, V.V., Swarup, S., Hoyer, M.J., Paulo, J.A., and Harper, J.W. (2021). Quantitative proteomics reveals the selectivity of ubiquitin-binding autophagy receptors in the turnover of damaged lysosomes by lysophagy. eLife *10*, e72328. 10.7554/eLife.72328.

27. Abe, A., Kelly, R., Kollmeyer, J., Hiraoka, M., Lu, Y., and Shayman, J.A. (2008). The secretion and uptake of lysosomal phospholipase A2 by alveolar macrophages. J. Immunol. Baltim. Md 1950 *181*, 7873–7881. 10.4049/jimmunol.181.11.7873.

28. Malik, N., Ferreira, B.I., Hollstein, P.E., Curtis, S.D., Trefts, E., Weiser Novak, S., Yu, J., Gilson, R., Hellberg, K., Fang, L., et al. (2023). Induction of lysosomal and mitochondrial biogenesis by AMPK phosphorylation of FNIP1. Science *380*, eabj5559. 10.1126/science.abj5559.

29. Torra, A., Parent, A., Cuadros, T., Rodríguez-Galván, B., Ruiz-Bronchal, E., Ballabio, A., Bortolozzi, A., Vila, M., and Bové, J. (2018). Overexpression of TFEB Drives a Pleiotropic Neurotrophic Effect and Prevents Parkinson's Disease-Related Neurodegeneration. Mol. Ther. *26*, 1552–1567. 10.1016/j.ymthe.2018.02.022.

30. Li, M., Khambu, B., Zhang, H., Kang, J.-H., Chen, X., Chen, D., Vollmer, L., Liu, P.-Q., Vogt, A., and Yin, X.-M. (2013). Suppression of Lysosome Function Induces Autophagy via a Feedback Down-regulation of MTOR Complex 1 (MTORC1) Activity*. J. Biol. Chem. *288*, 35769–35780. 10.1074/jbc.M113.511212.

31. McCauliff, L.A., Langan, A., Li, R., Ilnytska, O., Bose, D., Waghalter, M., Lai, K., Kahn, P.C., and Storch, J. Intracellular cholesterol trafficking is dependent upon NPC2 interaction with lysobisphosphatidic acid. eLife *8*, e50832. 10.7554/eLife.50832.

32. Ilnytska, O., Lai, K., Gorshkov, K., Schultz, M.L., Tran, B.N., Jeziorek, M., Kunkel, T.J., Azaria, R.D., McLoughlin, H.S., Waghalter, M., et al. (2021). Enrichment of NPC1-deficient cells with the lipid LBPA stimulates autophagy, improves lysosomal function, and reduces cholesterol storage. J. Biol. Chem. *297*. 10.1016/j.jbc.2021.100813.

33. Medoh, U.N., Hims, A., Chen, J.Y., Ghoochani, A., Nyame, K., Dong, W., and Abu-Remaileh, M. (2023). The Batten disease gene product CLN5 is the lysosomal

bis(monoacylglycero)phosphate synthase. Science *381*, 1182–1189. 10.1126/science.adg9288.

34. Body, D.R., and Gray, G.M. (1967). The isolation and characterisation of phosphatidylglycerol and a structural isomer from pig lung. Chem. Phys. Lipids *1*, 254–263. 10.1016/0009-3084(67)90032-1.

35. Anderson, D.M.G., Ablonczy, Z., Koutalos, Y., Hanneken, A.M., Spraggins, J.M., Calcutt, M.W., Crouch, R.K., Caprioli, R.M., and Schey, K.L. (2017). Bis(monoacylglycero)phosphate lipids in the retinal pigment epithelium implicate lysosomal/endosomal dysfunction in a model of Stargardt disease and human retinas. Sci. Rep. *7*, 17352. 10.1038/s41598-017-17402-1.

36. Hankin, J.A., Murphy, R.C., Barkley, R.M., and Gijón, M.A. (2015). Ion Mobility and Tandem Mass Spectrometry of Phosphatidylglycerol and Bis(monoacylglycerol)phosphate (BMP). Int. J. Mass Spectrom. *378*, 255–263. 10.1016/j.ijms.2014.08.026.

37. Scherer, M., Schmitz, G., and Liebisch, G. (2010). Simultaneous Quantification of Cardiolipin, Bis(monoacylglycero)phosphate and their Precursors by Hydrophilic Interaction LC−MS/MS Including Correction of Isotopic Overlap. Anal. Chem. *82*, 8794–8799. 10.1021/ac1021826.

38. Grabner, G.F., Fawzy, N., Schreiber, R., Pusch, L.M., Bulfon, D., Koefeler, H., Eichmann, T.O., Lass, A., Schweiger, M., Marsche, G., et al. (2020). Metabolic regulation of the lysosomal cofactor bis(monoacylglycero)phosphate in mice. J. Lipid Res. *61*, 995–1003. 10.1194/jlr.RA119000516.

39. Grabner, G.F., Fawzy, N., Pribasnig, M.A., Trieb, M., Taschler, U., Holzer, M., Schweiger, M., Wolinski, H., Kolb, D., Horvath, A., et al. (2019). Metabolic disease and ABHD6 alter the circulating bis(monoacylglycerol)phosphate profile in mice and humans. J. Lipid Res. *60*, 1020–1031. 10.1194/jlr.M093351.

40. Merchant, K.M., Simuni, T., Fedler, J., Caspell-Garcia, C., Brumm, M., Nudelman, K.N.H., Tengstrandt, E., Hsieh, F., Alcalay, R.N., Coffey, C., et al. (2023). LRRK2 and GBA1 variant carriers have higher urinary bis(monacylglycerol) phosphate concentrations in PPMI cohorts. Npj Park. Dis. *9*, 1–10. 10.1038/s41531-023-00468-2.

41. Boland, S., Swarup, S., Ambaw, Y.A., Malia, P.C., Richards, R.C., Fischer, A.W., Singh, S., Aggarwal, G., Spina, S., Nana, A.L., et al. (2022). Deficiency of the frontotemporal dementia gene GRN results in gangliosidosis. Nat. Commun. *13*, 5924. 10.1038/s41467-022-33500-9.

42. Logan, T., Simon, M.J., Rana, A., Cherf, G.M., Srivastava, A., Davis, S.S., Low, R.L.Y., Chiu, C.-L., Fang, M., Huang, F., et al. (2021). Rescue of a lysosomal storage disorder caused by Grn loss of function with a brain penetrant progranulin biologic. Cell *184*, 4651-4668.e25. 10.1016/j.cell.2021.08.002.

43. Chen, S., Francioli, L.C., Goodrich, J.K., Collins, R.L., Kanai, M., Wang, Q., Alföldi, J., Watts, N.A., Vittal, C., Gauthier, L.D., et al. (2022). A genome-wide mutational constraint map quantified from variation in 76,156 human genomes. 2022.03.20.485034. 10.1101/2022.03.20.485034.

44. Abe, A., Hiraoka, M., and Shayman, J.A. (2007). The acylation of lipophilic alcohols by lysosomal phospholipase A2. J. Lipid Res. *48*, 2255–2263. 10.1194/jlr.M700277-JLR200.

45. Taniyama, Y., Shibata, S., Kita, S., Horikoshi, K., Fuse, H., Shirafuji, H., Sumino, Y., and Fujino, M. (1999). Cloning and Expression of a Novel Lysophospholipase Which Structurally Resembles Lecithin Cholesterol Acyltransferase. Biochem. Biophys. Res. Commun. *257*, 50–56. 10.1006/bbrc.1999.0411.

46. Abe, A., Hiraoka, M., and Shayman, J.A. (2006). Positional specificity of lysosomal phospholipase A2. J. Lipid Res. *47*, 2268–2279. 10.1194/jlr.M600183-JLR200.

47. Hinkovska-Galcheva, V., Kelly, R., Manthei, K.A., Bouley, R., Yuan, W., Schwendeman, A., Tesmer, J.J.G., and Shayman, J.A. (2018). Determinants of pH profile and acyl chain selectivity in lysosomal phospholipase A2. J. Lipid Res. *59*, 1205–1218. 10.1194/jlr.M084012.

48. Glukhova, A., Hinkovska-Galcheva, V., Kelly, R., Abe, A., Shayman, J.A., and Tesmer, J.J.G. (2015). Structure and function of lysosomal phospholipase A2 and lecithin:cholesterol acyltransferase. Nat. Commun. *6*, 6250. 10.1038/ncomms7250.

49. Bouley, R.A., Hinkovska-Galcheva, V., Shayman, J.A., and Tesmer, J.J.G. (2019). Structural basis of lysosomal phospholipase A2 inhibition by Zn2+. Biochemistry *58*, 1709–1717. 10.1021/acs.biochem.8b01124.

50. Naquet, P., Kerr, E.W., Vickers, S.D., and Leonardi, R. (2020). Regulation of coenzyme A levels by degradation: the ‘Ins and Outs.’ Prog. Lipid Res. *78*, 101028. 10.1016/j.plipres.2020.101028.

51. Kagohashi, Y., Sasaki, M., May, A.I., Kawamata, T., and Ohsumi, Y. (2023). The mechanism of Atg15-mediated membrane disruption in autophagy. 2023.06.26.546516. 10.1101/2023.06.26.546516.

52. Li, Y., Wang, X., Li, M., Yang, C., and Wang, X. M05B5.4 (lysosomal phospholipase A2) promotes disintegration of autophagic vesicles to maintain C. elegans development. Autophagy *18*, 595–607. 10.1080/15548627.2021.1943178.

53. Chen, J., Cazenave-Gassiot, A., Xu, Y., Piroli, P., Hwang, R., DeFreitas, L., Chan, R.B., Di Paolo, G., Nandakumar, R., Wenk, M.R., et al. (2023). Lysosomal phospholipase A2 contributes to the biosynthesis of the atypical late endosome lipid bis(monoacylglycero)phosphate. Commun. Biol. *6*, 1–11. 10.1038/s42003-023-04573-z.

54. Else, P.L. (2020). The highly unnatural fatty acid profile of cells in culture. Prog. Lipid Res. *77*, 101017. 10.1016/j.plipres.2019.101017.

55. Chao, X., Wang, S., Hlobik, M., Ballabio, A., Ni, H.-M., and Ding, W.-X. (2022). Loss of Hepatic Transcription Factor EB Attenuates Alcohol-Associated Liver Carcinogenesis. Am. J. Pathol. *192*, 87–103. 10.1016/j.ajpath.2021.10.004.

56. Peng, B., Kopczynski, D., Pratt, B.S., Ejsing, C.S., Burla, B., Hermansson, M., Benke, P.I., Tan, S.H., Chan, M.Y., Torta, F., et al. (2020). LipidCreator workbench to probe the lipidomic landscape. Nat. Commun. *11*, 2057. 10.1038/s41467-020-15960-z.

57. Abe, A., Kelly, R., and Shayman, J.A. (2010). The measurement of lysosomal phospholipase A2 activity in plasma. J. Lipid Res. *51*, 2464–2470. 10.1194/jlr.D007146.

Figure 1

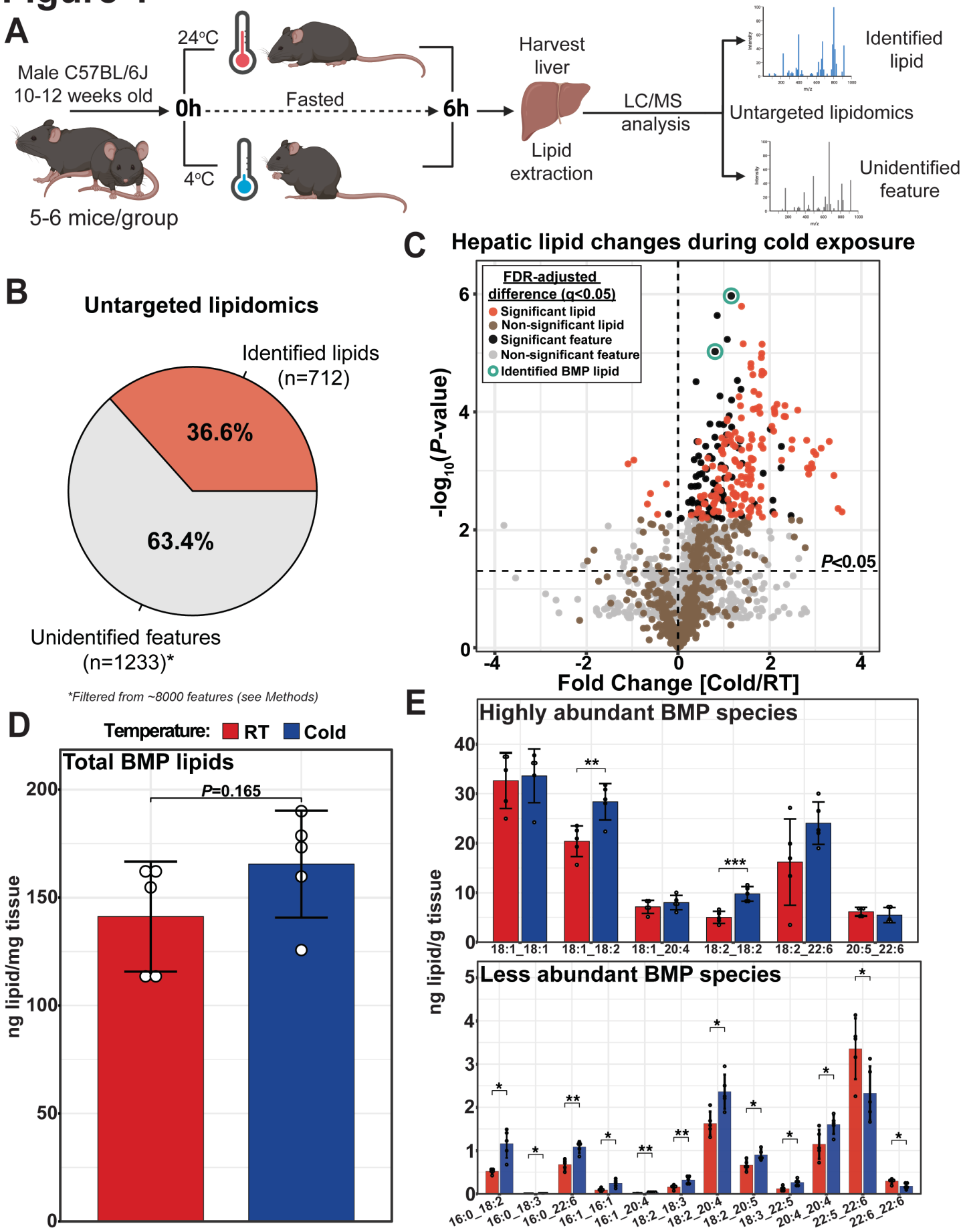
A
Male C57BL/6J
10-12 weeks old
5-6 mice/group
24°C
4°C
0h
Fasted
6h
Harvest
liver
Lipid
extraction
LC/MS
analysis
Identified
lipid
Untargeted lipidomics
Unidentified
feature
B
Untargeted lipidomics
Identified lipids
(n=712)
36.6%
63.4%
Unidentified features
(n=1233)*
*Filtered from ~8000 features (see Methods)
C
Hepatic lipid changes during cold exposure
FDR-adjusted
difference (q<0.05)
Significant lipid
Non-significant lipid
Significant feature
Non-significant feature
Identified BMP lipid
-log10(P-value)
P<0.05
Fold Change [Cold/RT]
D
Temperature: RT Cold
Total BMP lipids
P=0.165
ng lipid/mg tissue
E
Highly abundant BMP species
18:1_18:1
18:1_18:2
18:1_20:4
18:2_18:2
18:2_22:6
20:5_22:6
Less abundant BMP species
ng lipid/g tissue
16:0_18:2
16:0_18:3
16:0_22:6
16:1_16:1
16:1_20:4
18:2_18:3
18:2_20:4
18:2_20:5
18:3_22:5
20:4_20:4
22:5_22:6
22:6_22:6

Figure 2

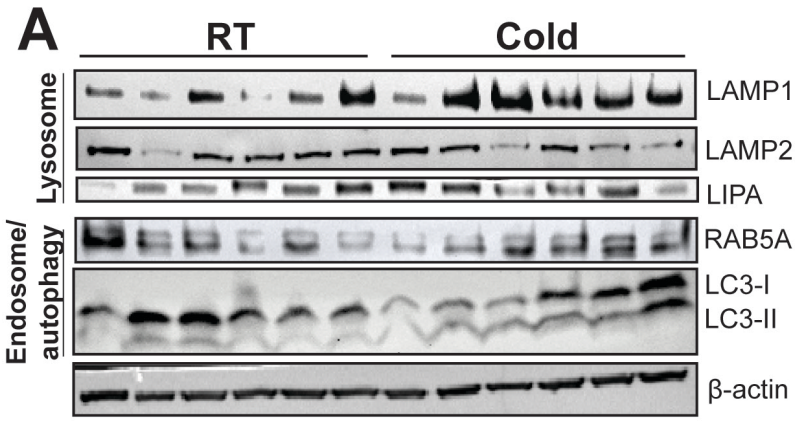
A
RT
Cold
Lysosome
LAMP1
LAMP2
LIPA
Endosome/ autophagy
RAB5A
LC3-I
LC3-II
β-actin

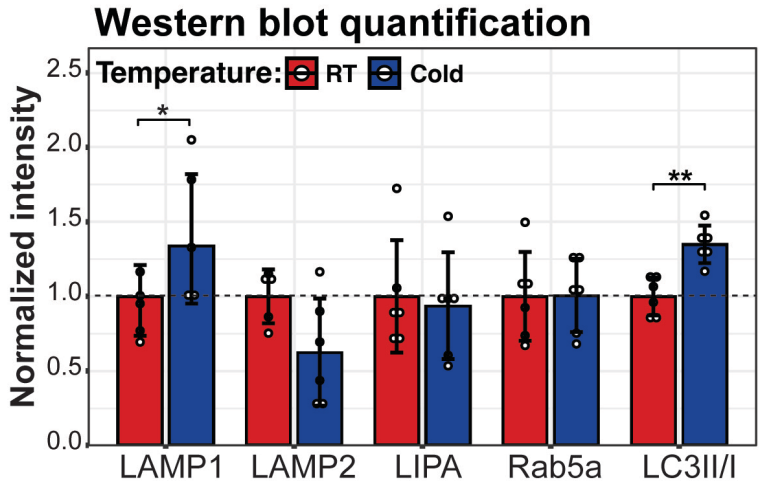
Western blot quantification
Temperature: RT Cold
Normalized intensity
2.5
2.0
1.5
1.0
0.5
0.0
*
**
LAMP1
LAMP2
LIPA
Rab5a
LC3II/I

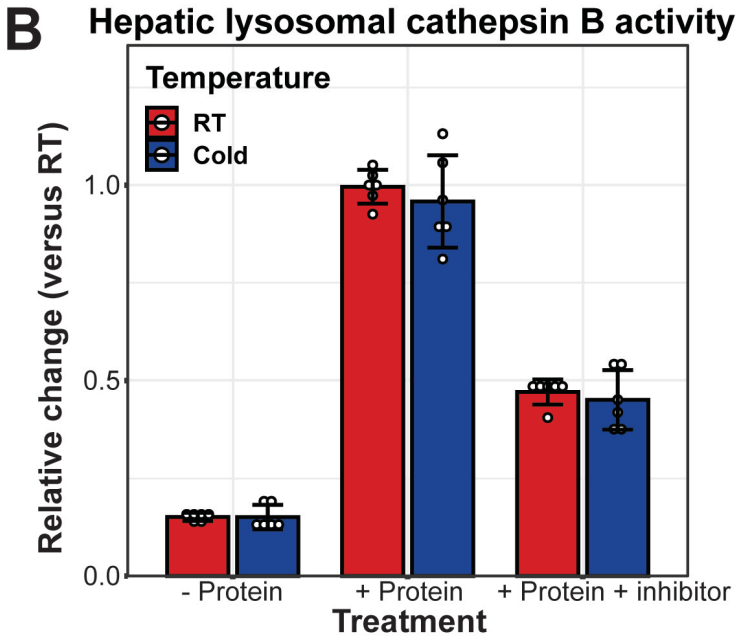
B
Hepatic lysosomal cathepsin B activity
Temperature
RT
Cold
Relative change (versus RT)
1.0
0.5
0.0
- Protein
+ Protein
+ Protein + inhibitor
Treatment

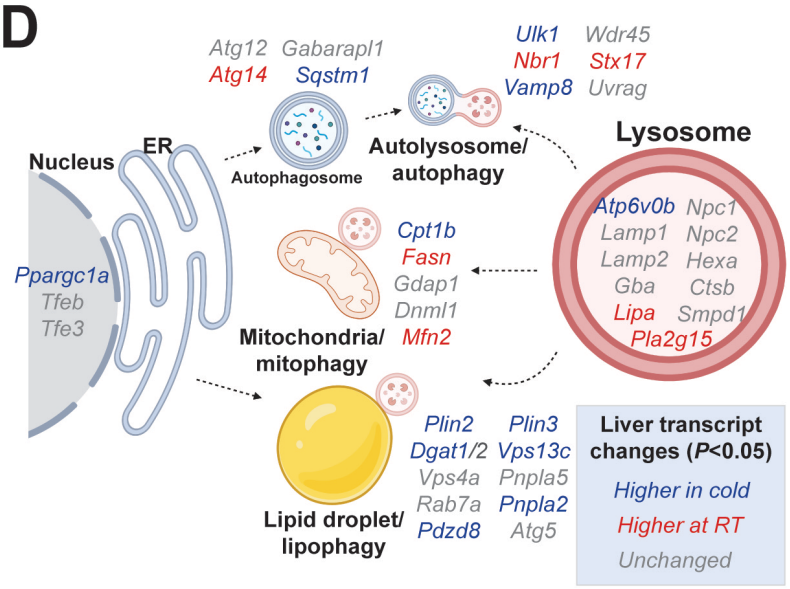
D
Atg12 Gabarapl1
Atg14 Sqstm1
Autophagosome
Ulk1 Wdr45
Nbr1 Stx17
Vamp8 Uvrag
Autolysosome/ autophagy
Lysosome
Nucleus
ER
Ppargc1a
Tfeb
Tfe3
Cpt1b
Fasn
Gdap1
Dnml1
Mfn2
Mitochondria/ mitophagy
Atp6v0b Npc1
Lamp1 Npc2
Lamp2 Hexa
Gba Ctsb
Lipa Smpd1
Pla2g15
Plin2 Plin3
Dgat1/2 Vps13c
Vps4a Pnpla5
Rab7a Pnpla2
Pdzd8 Atg5
Lipid droplet/ lipophagy
Liver transcript changes (P<0.05)
Higher in cold
Higher at RT
Unchanged

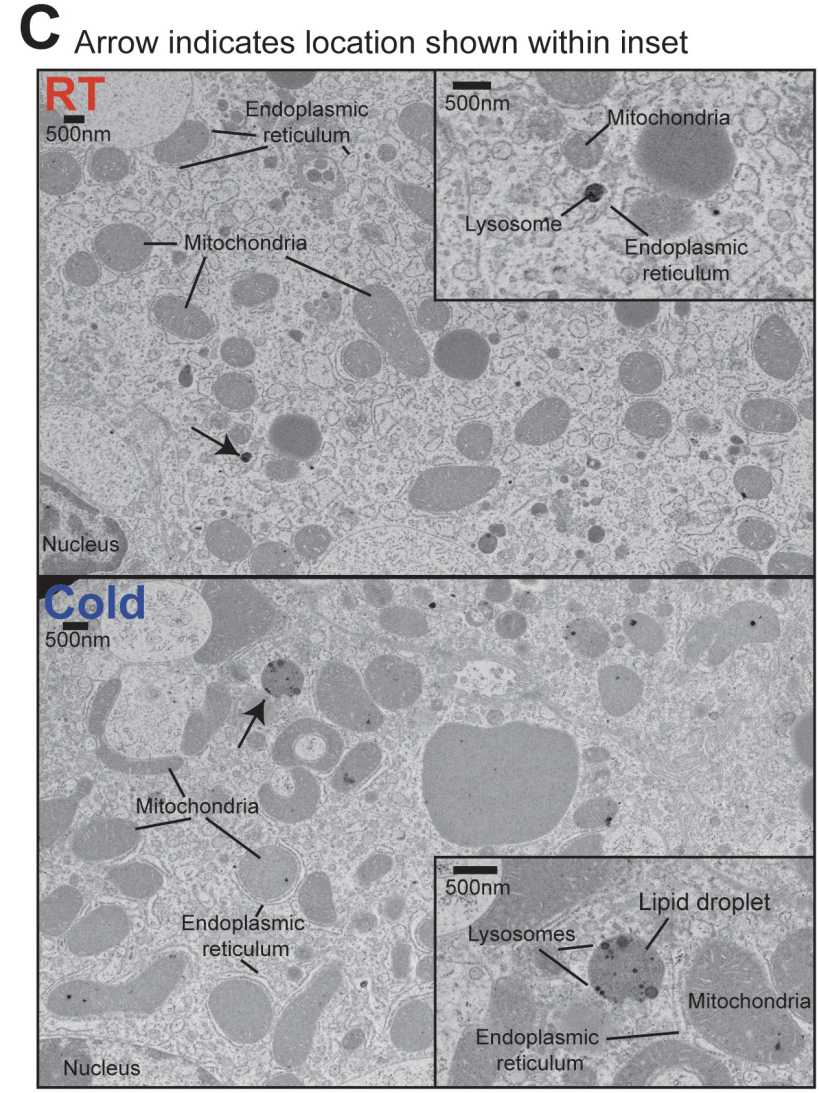
C
Arrow indicates location shown within inset
RT
500nm
Endoplasmic reticulum
Mitochondria
Nucleus
500nm
Mitochondria
Lysosome
Endoplasmic reticulum
Cold
500nm
Mitochondria
Endoplasmic reticulum
Nucleus
500nm
Lipid droplet
Lysosomes
Mitochondria
Endoplasmic reticulum

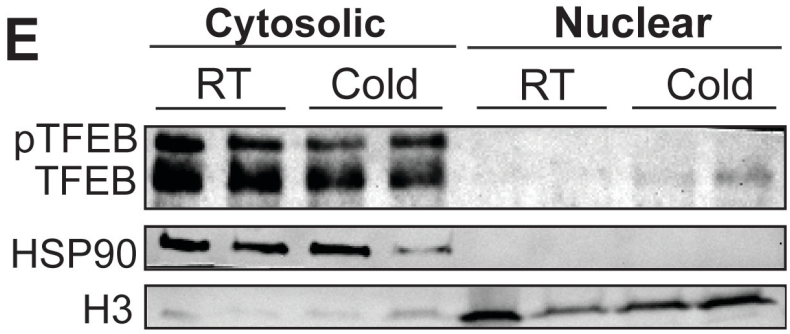
E
Cytosolic
Nuclear
RT
Cold
RT
Cold
pTFEB
TFEB
HSP90
H3

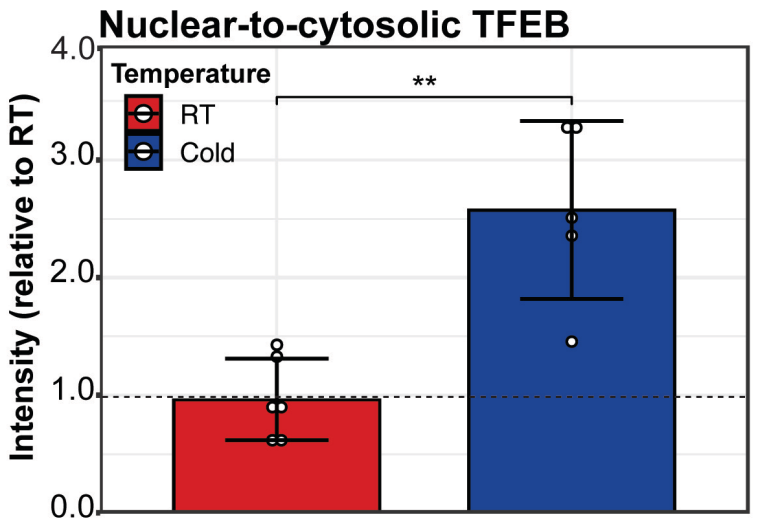
Nuclear-to-cytosolic TFEB
Temperature
RT
Cold
**
Intensity (relative to RT)
4.0
3.0
2.0
1.0
0.0

Figure 3

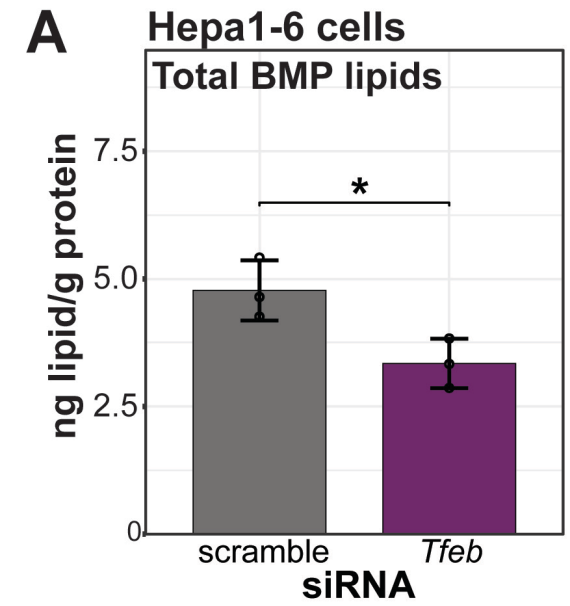
A
Hepa1-6 cells
Total BMP lipids
ng lipid/g protein
7.5
5.0
2.5
0
*
scramble
Tfeb
siRNA

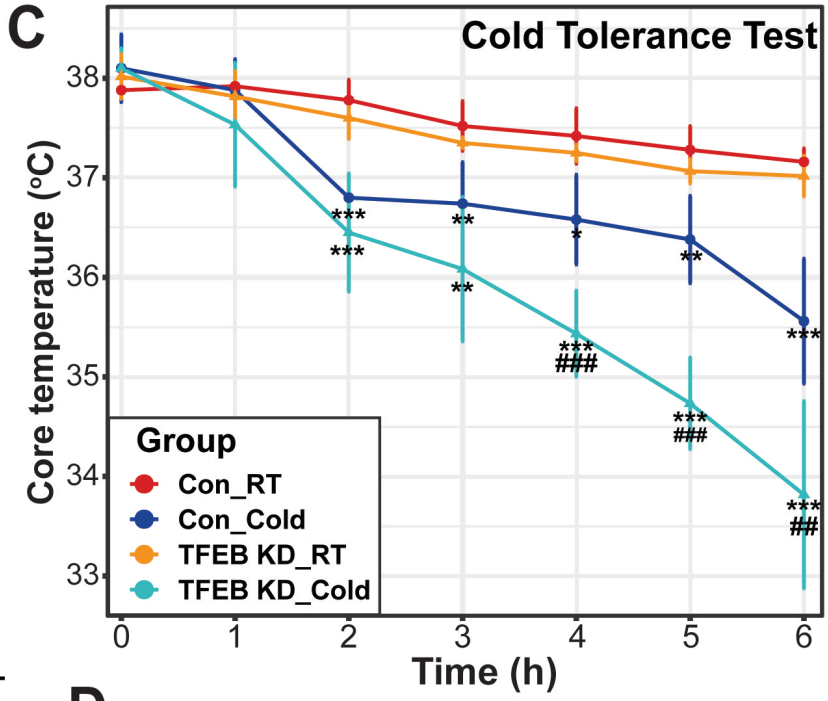
C
Cold Tolerance Test
Core temperature (°C)
38
37
36
35
34
33
Group
Con_RT
Con_Cold
TFEB KD_RT
TFEB KD_Cold
0
1
2
3
4
5
6
Time (h)

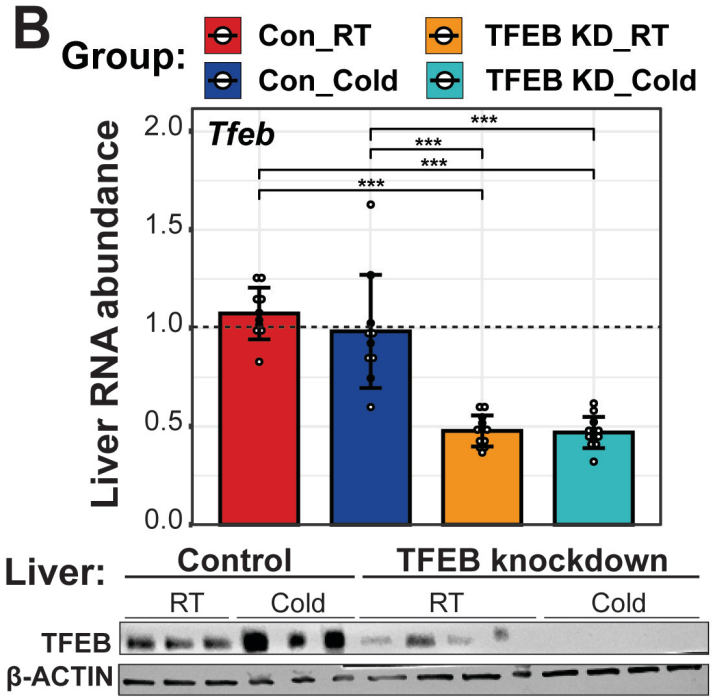
B
Group:
Con_RT
Con_Cold
TFEB KD_RT
TFEB KD_Cold
Tfeb
Liver RNA abundance
2.0
1.5
1.0
0.5
0.0
Liver:
Control
TFEB knockdown
RT
Cold
RT
Cold
TFEB
β-ACTIN

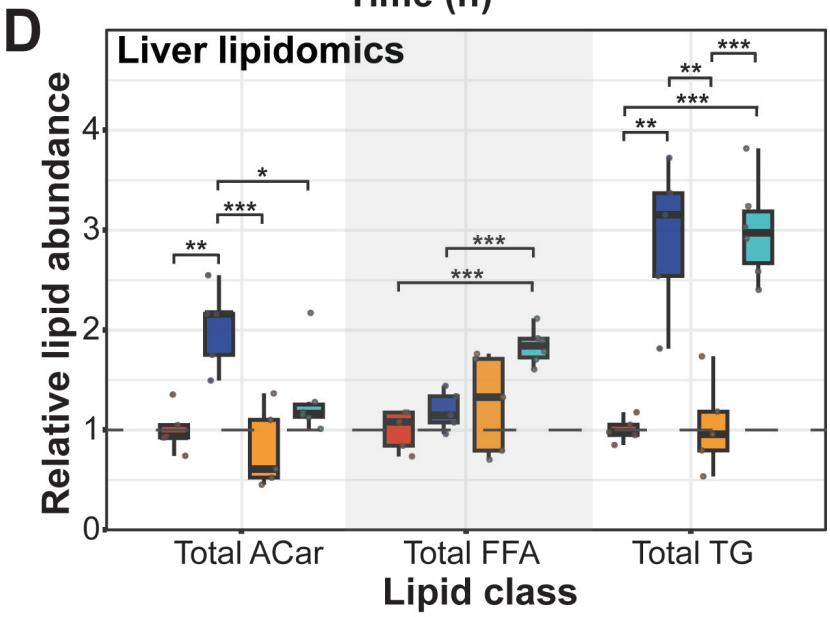
D
Liver lipidomics
Relative lipid abundance
4
3
2
1
0
Total ACar
Total FFA
Total TG
Lipid class

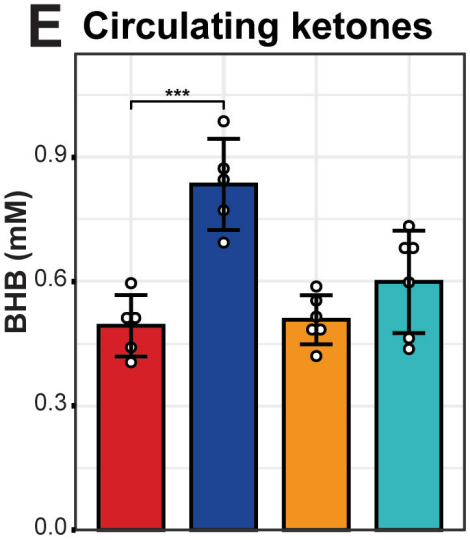
E
Circulating ketones
BHB (mM)
0.9
0.6
0.3
0.0

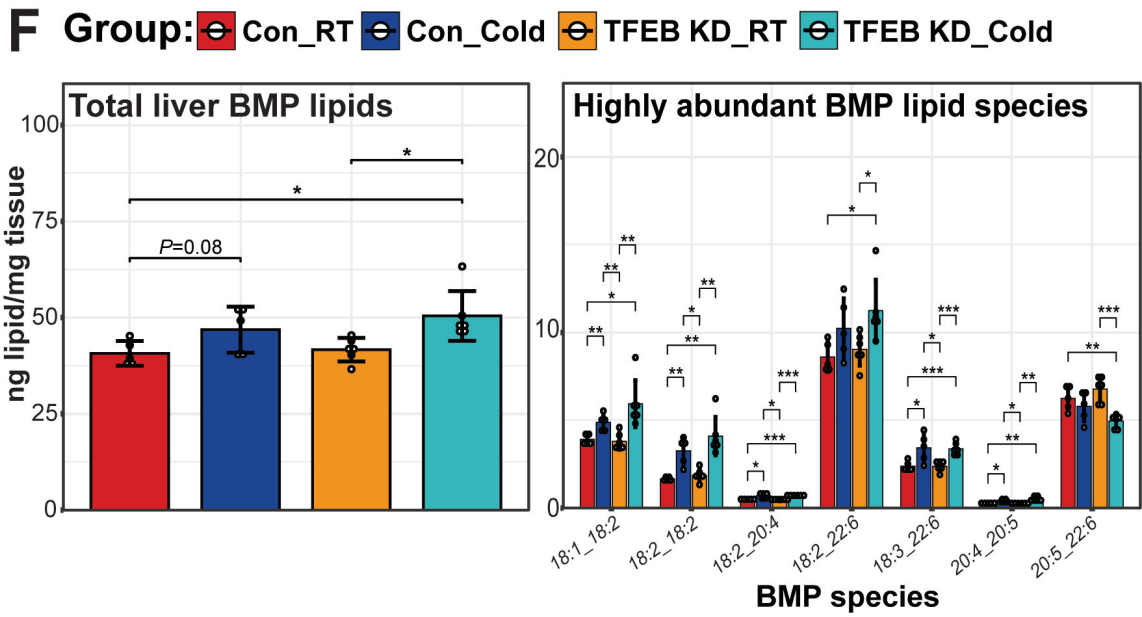
F
Group:
Con_RT
Con_Cold
TFEB KD_RT
TFEB KD_Cold
Total liver BMP lipids
ng lipid/mg tissue
100
75
50
25
0
P=0.08
Highly abundant BMP lipid species
20
10
0
18:1_18:2
18:2_18:2
18:2_20:4
18:2_22:6
18:3_22:6
20:4_20:5
20:5_22:6
BMP species

Figure 4

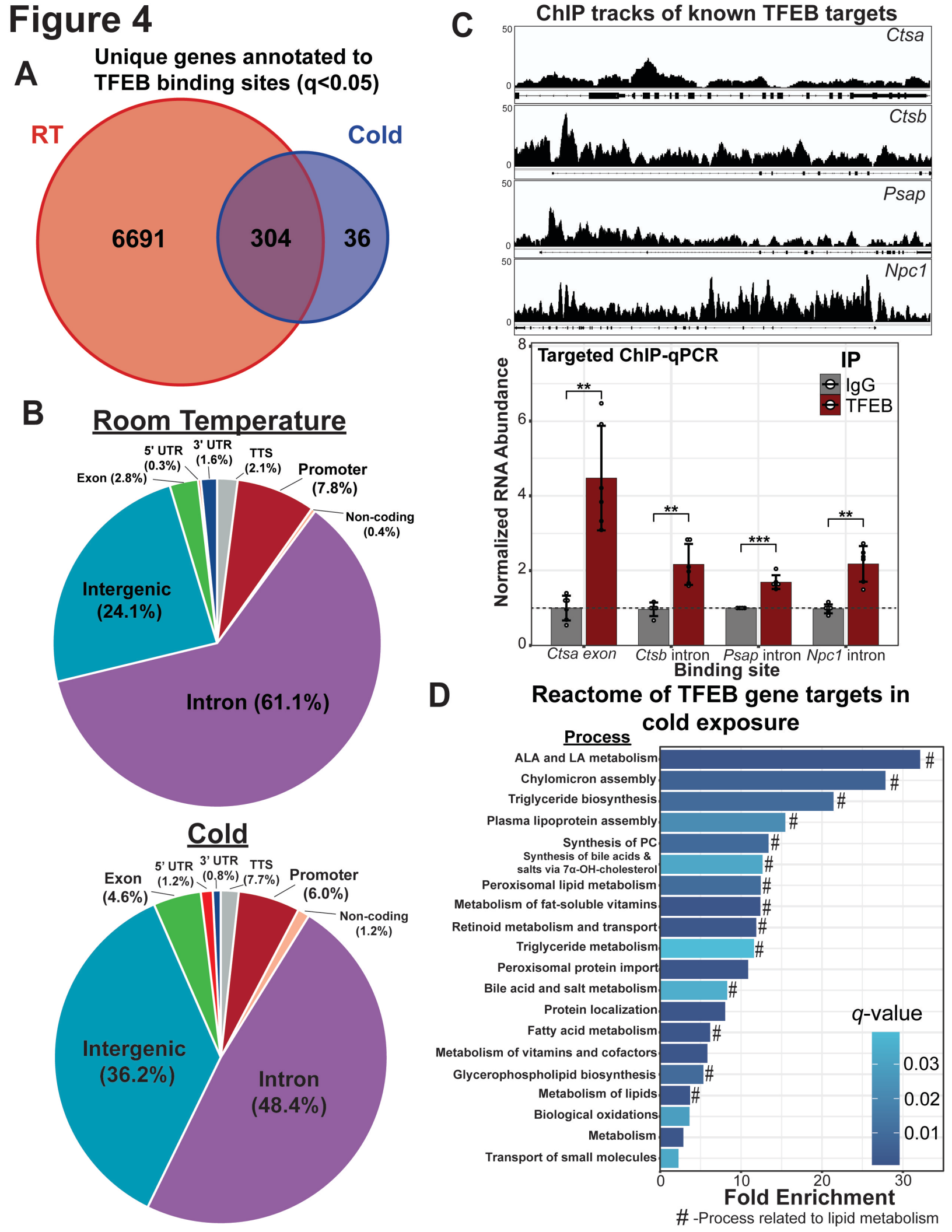
A
Unique genes annotated to TFEB binding sites (q<0.05)
RT
Cold
6691
304
36
B
Room Temperature
5' UTR (0.3%)
3' UTR (1.6%)
TTS (2.1%)
Promoter (7.8%)
Exon (2.8%)
Non-coding (0.4%)
Intergenic (24.1%)
Intron (61.1%)
Cold
Exon (4.6%)
5' UTR (1.2%)
3' UTR (0.8%)
TTS (7.7%)
Promoter (6.0%)
Non-coding (1.2%)
Intergenic (36.2%)
Intron (48.4%)
C
ChIP tracks of known TFEB targets
Ctsa
Ctsb
Psap
Npc1
Targeted ChIP-qPCR
IP
IgG
TFEB
Normalized RNA Abundance
Ctsa exon
Ctsb intron
Psap intron
Npc1 intron
Binding site
D
Reactome of TFEB gene targets in cold exposure
Process
ALA and LA metabolism
Chylomicron assembly
Triglyceride biosynthesis
Plasma lipoprotein assembly
Synthesis of PC
Synthesis of bile acids & salts via 7α-OH-cholesterol
Peroxisomal lipid metabolism
Metabolism of fat-soluble vitamins
Retinoid metabolism and transport
Triglyceride metabolism
Peroxisomal protein import
Bile acid and salt metabolism
Protein localization
Fatty acid metabolism
Metabolism of vitamins and cofactors
Glycerophospholipid biosynthesis
Metabolism of lipids
Biological oxidations
Metabolism
Transport of small molecules
q-value
Fold Enrichment
-Process related to lipid metabolism

Figure 5

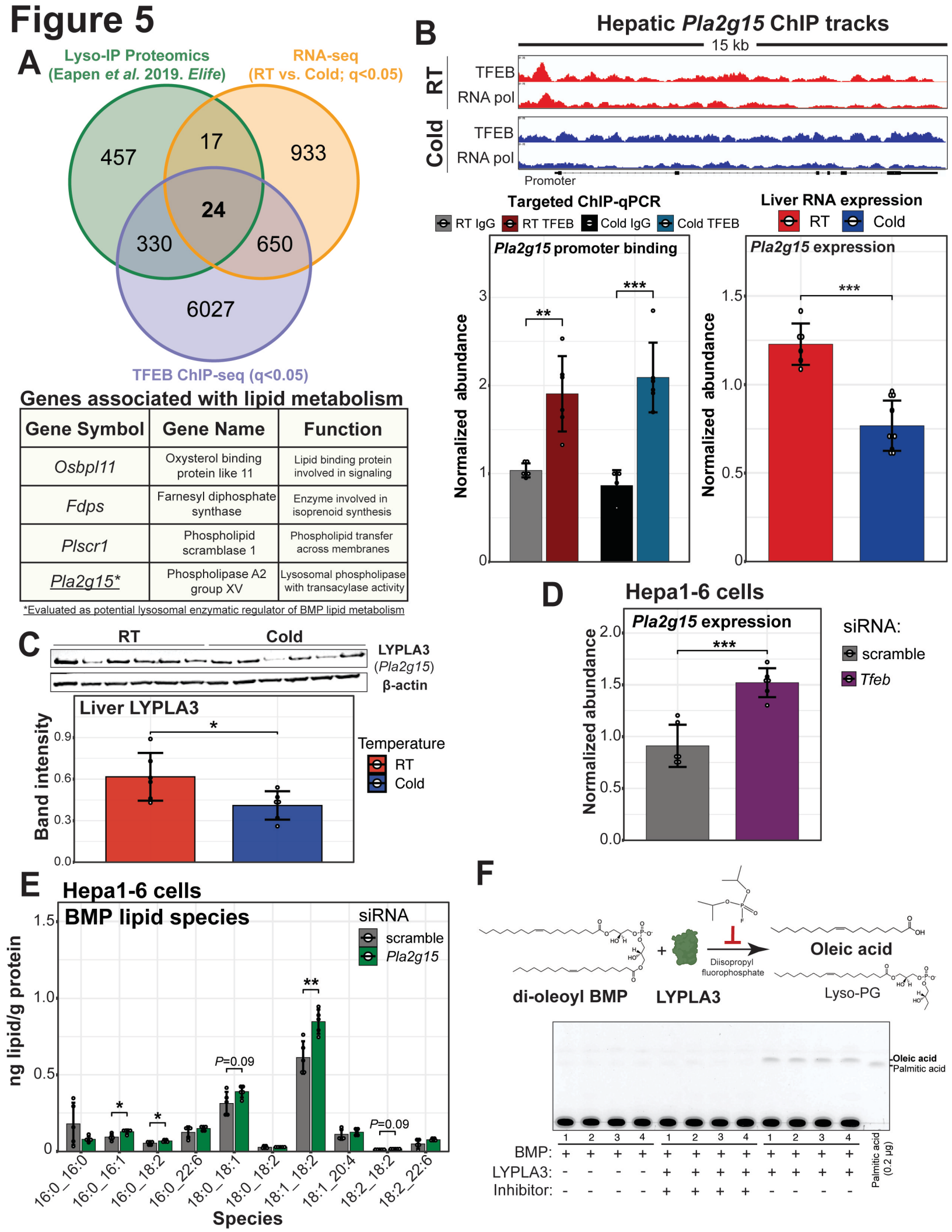

Genes associated with lipid metabolism

Gene Symbol	Gene Name	Function
Osbpl11	Oxysterol binding protein like 11	Lipid binding protein involved in signaling
Fdps	Farnesyl diphosphate synthase	Enzyme involved in isoprenoid synthesis
Plscr1	Phospholipid scramblase 1	Phospholipid transfer across membranes
*Pla2g15**	Phospholipase A2 group XV	Lysosomal phospholipase with transacylase activity

*Evaluated as potential lysosomal enzymatic regulator of BMP lipid metabolism

Supplementary Figure 1

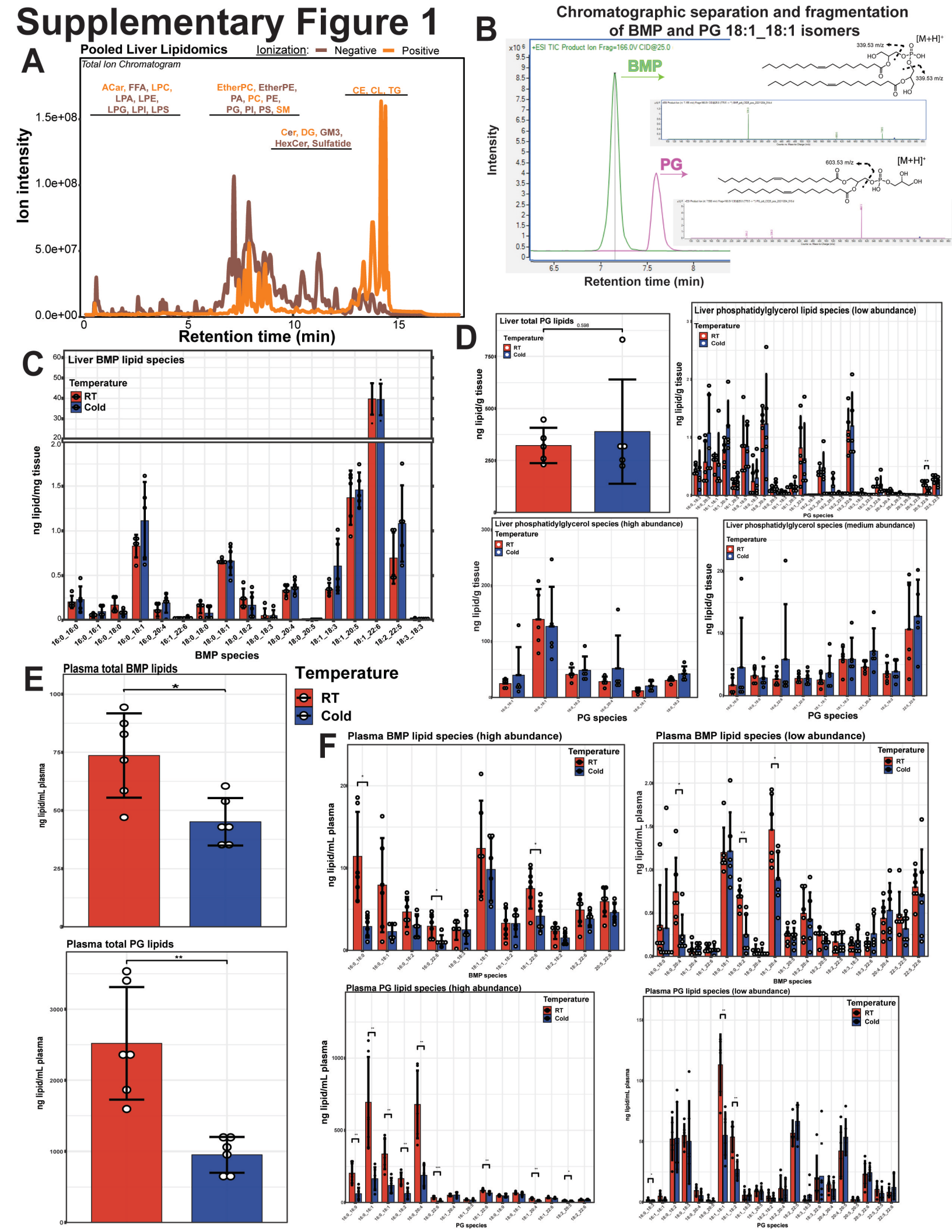

Supplementary Figure 2

A Liver gene expression

Temperature: RT Cold

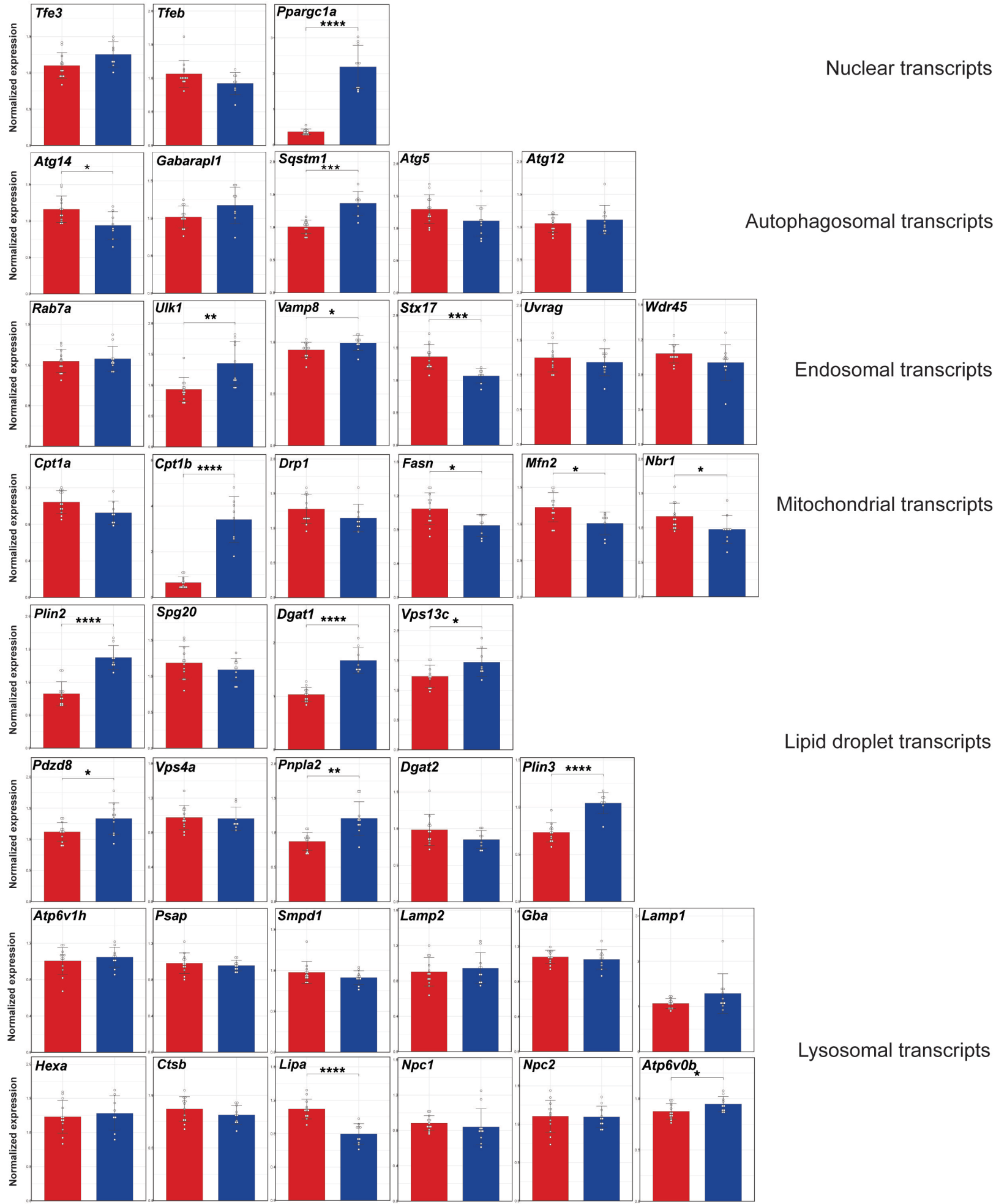

Supplementary Figure 3

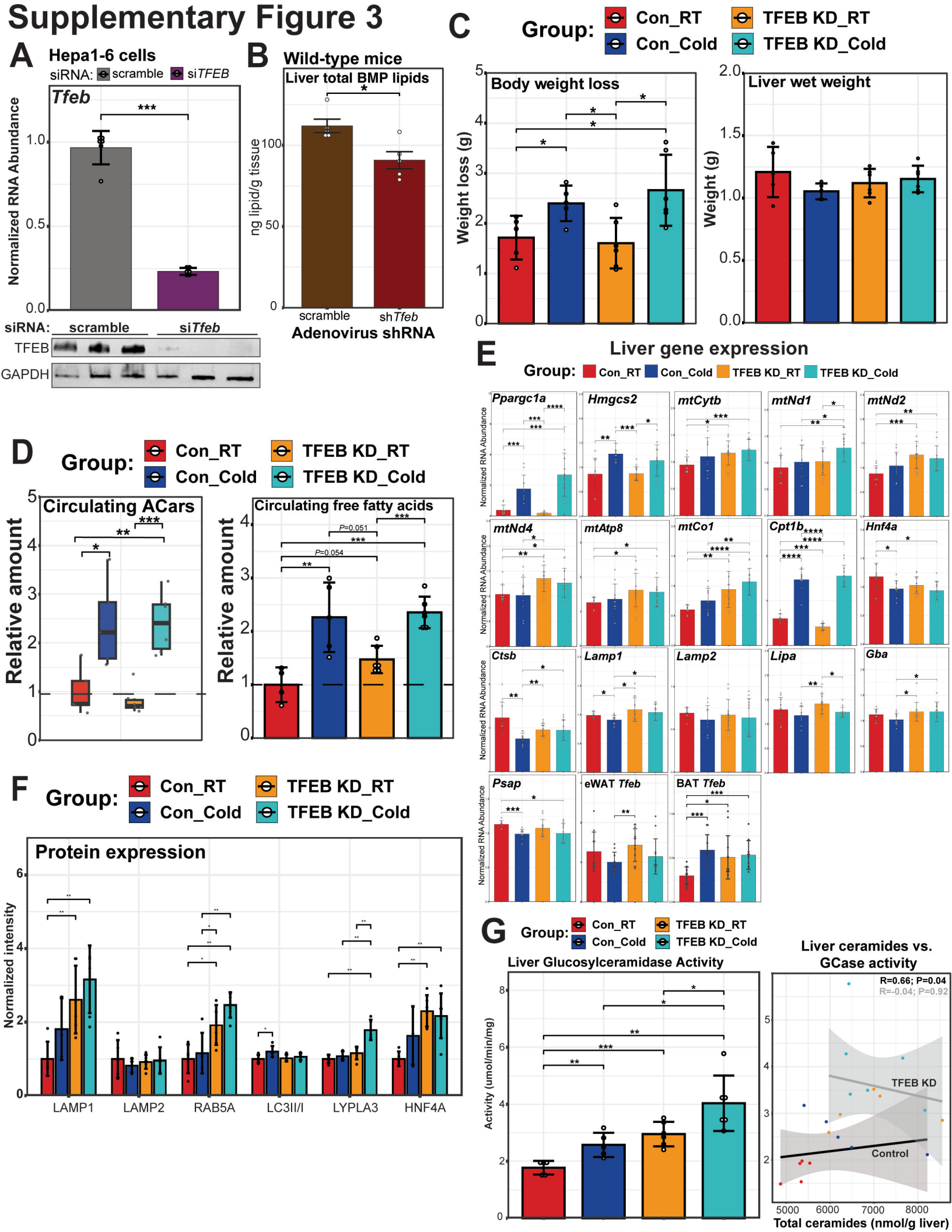

Supplementary Figure 4

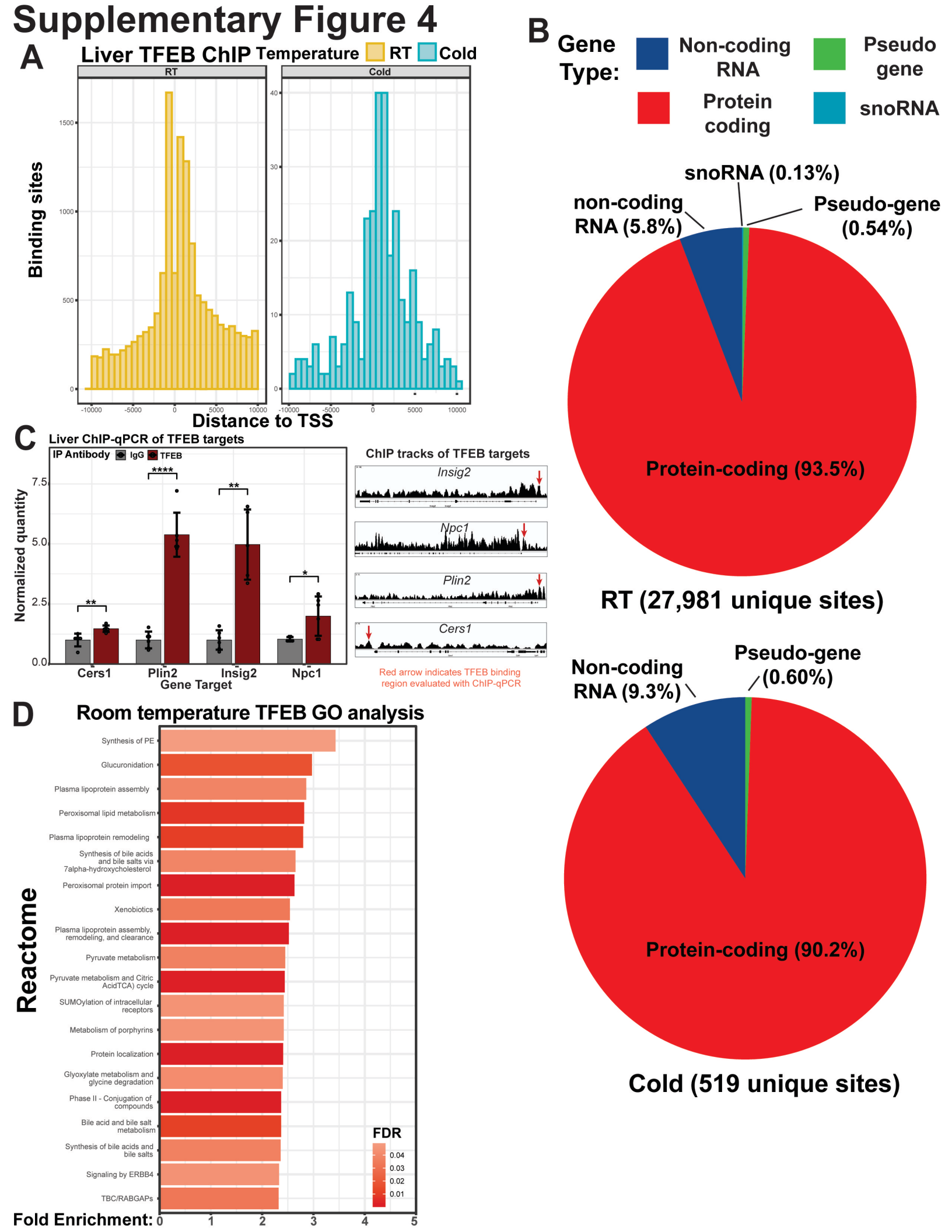
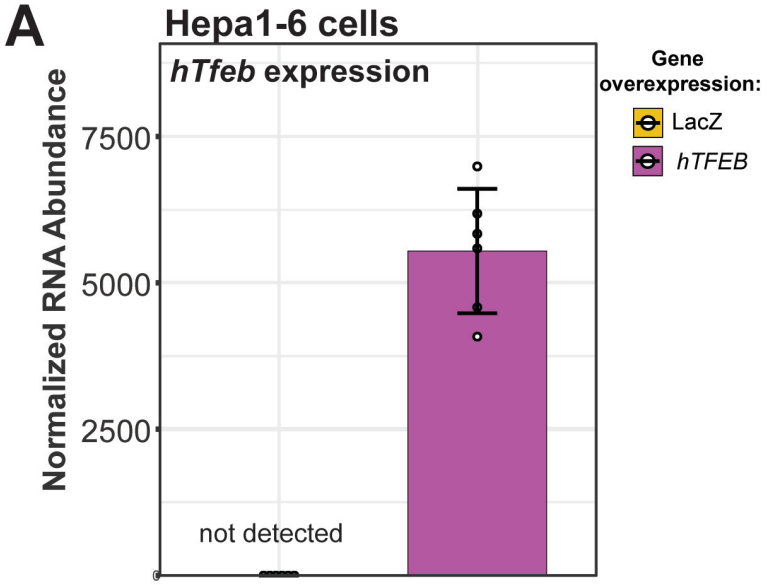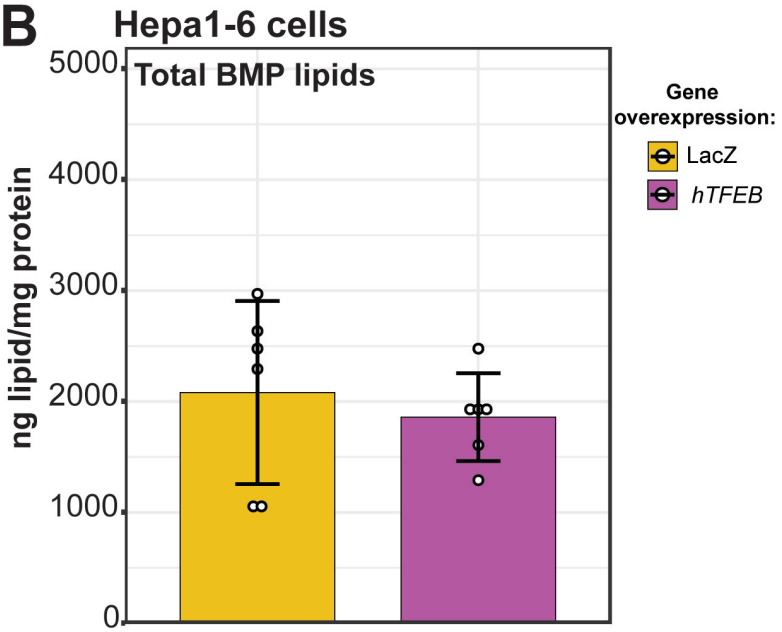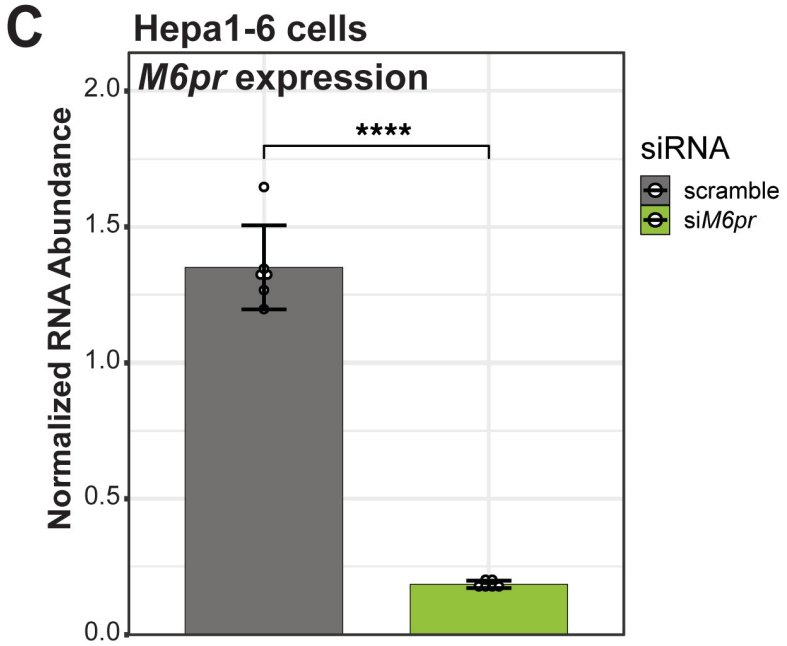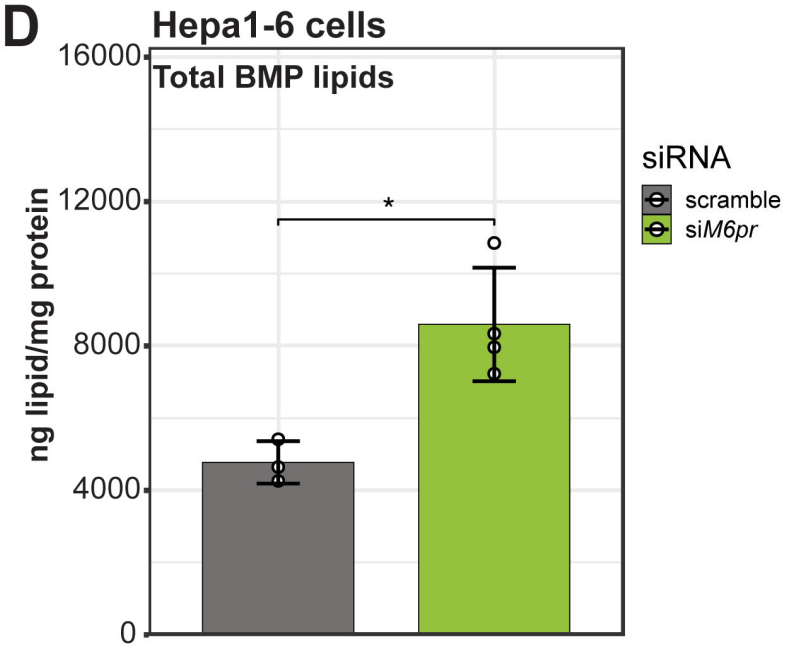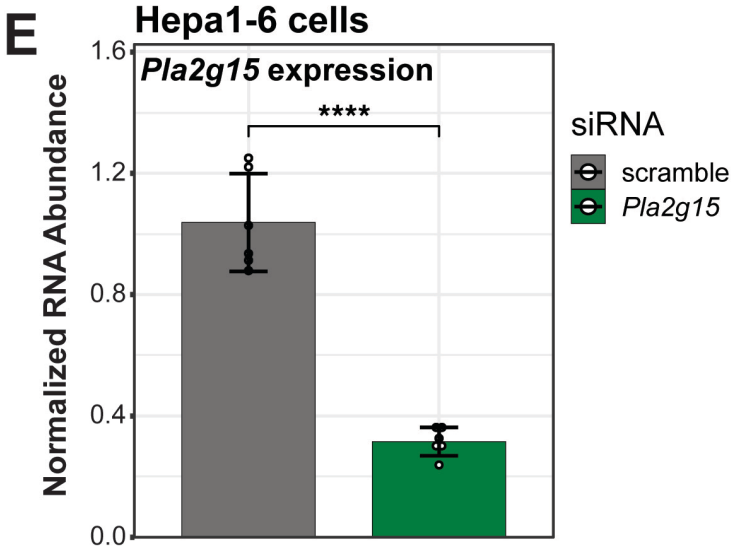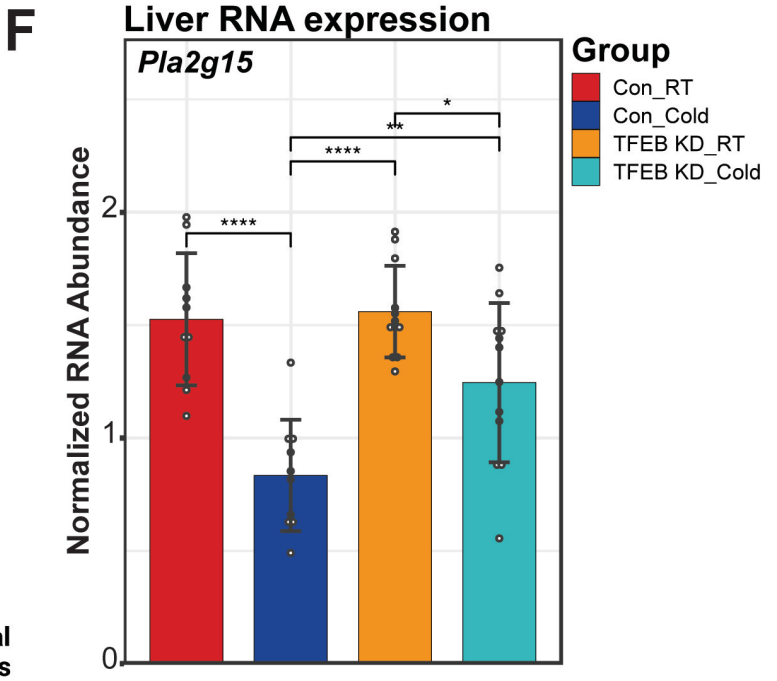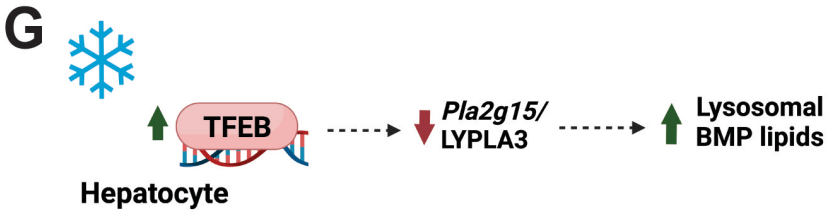
Supplementary Figure 5